4. Conclusions

The BASO-WX and BASO-WY values obtained from automated hematology analyzer XE-5000 could help to detect Jordans' anomaly. A notification system using an automated hematology analyzer may prompt the earlier and easier diagnosis of homozygous ATGL deficiency.

Acknowledgments

The authors would like to thank Dr. Toshimitsu Hamasaki for giving us valuable advice on statistical analysis. This work is supported by a research grant for rare and intractable diseases from the Ministry of Health, Labour, and Welfare of Japan. Y.O., A.W. and Y.S. are employees of Sysmex Corporation.

References

[1] C. Bruno, S. Dimauro, Lipid storage myopathies, Curr. Opin. Neurol. 21 (2008) 601–606, http://dx.doi.org/10.1097/WCO.0b013e32830dd5a6.
[2] P. Laforêt, C. Vianey-Saban, Disorders of muscle lipid metabolism: diagnostic and therapeutic challenges, Neuromuscul. Disord. 20 (2010) 693–700, http://dx.doi.org/10.1016/j.nmd.2010.06.018.
[3] J. Fischer, C. Lefèvre, E. Morava, J.M. Mussini, P. Laforêt, A. Negre-Salvayre, M. Lathrop, R. Salvayre, The gene encoding adipose triglyceride lipase (PNPLA2) is mutated in neutral lipid storage disease with myopathy, Nat. Genet. 39 (2007) 28–30, http://dx.doi.org/10.1038/ng1951.
[4] M. Akiyama, K. Sakai, M. Ogawa, J.R. McMillan, D. Sawamura, H. Shimizu, Novel duplication mutation in the patatin domain of adipose triglyceride lipase (PNPLA2) in neutral lipid storage disease with severe myopathy, Muscle Nerve 36 (2007) 856–859, http://dx.doi.org/10.1002/mus.20869.
[5] K. Kobayashi, T. Inoguchi, Y. Maeda, N. Nakashima, A. Kuwano, E. Eto, N. Ueno, S. Sasaki, F. Sawada, M. Fujii, Y. Matoba, S. Sumiyoshi, H. Kawate, R. Takayanagi, The lack of the C-terminal domain of adipose triglyceride lipase causes neutral lipid storage disease through impaired interactions with lipid droplets, J. Clin. Endocrinol. Metab. 93 (2008) 2877–2884, http://dx.doi.org/10.1210/jc.2007-2247.
[6] K. Hirano, Y. Ikeda, N. Zaima, Y. Sakata, G. Matsumiya, Triglyceride deposit cardiomyovasculopathy, N. Engl. J. Med. 359 (2008) 2396–2398, http://dx.doi.org/10.1056/NEJMc0805305.
[7] K. Hirano, A novel clinical entity: triglyceride deposit cardiomyovasculopathy, J. Atheroscler. Thromb. 16 (2009) 702–705, http://dx.doi.org/10.5551/jat.1669.
[8] K. Hirano, T. Tanaka, Y. Ikeda, S. Yamaguchi, N. Zaima, K. Kobayashi, A. Suzuki, Y. Sakata, Y. Sakata, K. Kobayashi, T. Toda, N. Fukushima, H. Ishibashi-Ueda, D. Tavian, H. Nagasaka, S.P. Hui, H. Chiba, Y. Sawa, M. Hori, Genetic mutations in adipose triglyceride lipase and myocardial up-regulation of peroxisome proliferated activated receptor-gamma in patients with triglyceride deposit cardiomyovasculopathy, Biochem. Biophys. Res. Commun. 443 (2014) 574–579, http://dx.doi.org/10.1016/j.bbrc.2013.12.003.
[9] P. Reilich, R. Horvath, S. Krause, N. Schramm, D.M. Turnbull, M. Trenell, K.G. Hollingsworth, G.S. Gorman, V.H. Hans, J. Reimann, A. MacMillan, L. Turner, A. Schollen, G. Witte, B. Czermin, E. Holinski-Feder, M.C. Walter, B. Schoser, H. Lochmüller, The phenotypic spectrum of neutral lipid storage myopathy due to mutations in the PNPLA2 gene, J. Neurol. 258 (2011) 1987–1997, http://dx.doi.org/10.1007/s00415-011-6055-4.
[10] D. Tavian, S. Missaglia, C. Redaelli, E.M. Pennisi, G. Invernici, R. Wessalowski, R. Maiwald, M. Arca, R.A. Coleman, Contribution of novel ATGL missense mutations to the clinical phenotype of NLSD-M: a strikingly low amount of lipase activity may preserve cardiac function, Hum. Mol. Genet. 21 (2012) 5318–5328, http://dx.doi.org/10.1093/hmg/dds388.
[11] K. Kaneko, H. Kuroda, R. Izumi, M. Tateyama, M. Kato, K. Sugimura, Y. Sakata, Y. Ikeda, K. Hirano, M. Aoki, A novel mutation in PNPLA2 causes neutral lipid storage disease with myopathy and triglyceride deposit cardiomyovasculopathy: a case report and literature review. Neuromuscul. Disord. (in press). http://dx.doi.org/10.1016/j.nmd.2014.04.001 .
[12] H.O. Akman, G. Davidzon, K. Tanji, E.J. Macdermott, L. Larsen, M.M. Davidson, R.G. Haller, L.S. Szczepaniak, T.J. Lehman, M. Hirano, S. DiMauro, Neutral lipid storage disease with subclinical myopathy due to a retrotransposal insertion in the PNPLA2 gene, Neuromuscul. Disord. 20 (2010) 397–402, http://dx.doi.org/10.1016/j.nmd.2010.04.004.
[13] L. Perrin, L. Féasson, A. Furby, P. Laforêt, F.M. Petit, V. Gautheron, S. Chabrier, PNPLA2 mutation: a paediatric case with early onset but indolent course, Neuromuscul. Disord. 23 (2013) 986–991, http://dx.doi.org/10.1016/j.nmd.2013.08.008.
[14] K. Tauchi-Sato, S. Ozeki, T. Houjou, R. Taguchi, T. Fujimoto, The surface of lipid droplets is a phospholipid monolayer with a unique fatty acid composition, J. Biol. Chem. 277 (2002) 44507–44512, http://dx.doi.org/10.1074/jbc.M207712200.
[15] R.Y. Wang, O.A. Bodamer, M.S. Watson, W.R. Wilcox, ACMG Work Group on Diagnostic Confirmation of Lysosomal Storage Diseases: diagnostic confirmation and management of presymptomatic individuals, Genet. Med. 13 (2011) 457–484, http://dx.doi.org/10.1097/GIM.0b013e318211a7e1.
[16] M.C. Janssen, B. van Engelen, L. Kapusta, M. Lammens, M. van Dijk, J. Fischer, M. van der Graaf, R.A. Wevers, M. Fahrleitner, R. Zimmermann, E. Morava, Symptomatic lipid storage in carriers for the PNPLA2 gene, Eur. J. Hum. Genet. 21 (2013) 807–815, http://dx.doi.org/10.1038/ejhg.2012.256.
[17] C. Lefèvre, F. Jobard, F. Caux, B. Bouadjar, A. Karaduman, R. Heilig, H. Lakhdar, A. Wollenberg, J.L. Verret, J. Weissenbach, M. Ozguc, M. Lathrop, J.F. Prud'homme, J. Fischer, Mutations in CGI-58, the gene encoding a new protein of the esterase/lipase/thioesterase subfamily, in Chanarin–Dorfman syndrome, Am. J. Hum. Genet. 69 (2001) 1002–1012, http://dx.doi.org/10.1086/324121.
[18] C. Bruno, E. Bertini, M. Di Rocco, D. Cassandrini, G. Ruffa, T. De Toni, M. Seri, M. Spada, G. Li Volti, A. D'Amico, F. Trucco, M. Arca, C. Casali, C. Angelini, S. Dimauro, C. Minetti, Clinical and genetic characterization of Chanarin–Dorfman syndrome, Biochem. Biophys. Res. Commun. 369 (2008) 1125–1128, http://dx.doi.org/10.1016/j.bbrc.2008.03.010.
[19] J.P. Bonnefont, F. Demaugre, C. Prip-Buus, J.M. Saudubray, M. Brivet, N. Abadi, L. Thuillier, Carnitine palmitoyltransferase deficiencies, Mol. Genet. Metab. 68 (1999) 424–440, http://dx.doi.org/10.1006/mgme.1999.2938.

Molecular Genetics and Metabolism Reports 1 (2014) 264–268

Contents lists available at ScienceDirect

Molecular Genetics and Metabolism Reports

journal homepage: http://www.journals.elsevier.com/molecular-genetics-and-metabolism-reports/

Short Communication

Disease-associated marked hyperalphalipoproteinemia

Ken-ichi Hirano [a,*,1], Hironori Nagasaka [b,1], Kazuhiro Kobayashi [c], Satoshi Yamaguchi [a], Akira Suzuki [a], Tatsushi Toda [c], Manabu Doyu [d]

[a] Laboratory of Cardiovascular Disease, Novel, Non-invasive, and Nutritional Therapeutics (CNT), Graduate School of Medicine, Osaka University, Osaka 565-0874, Japan
[b] Department of Pediatrics, Takarazuka City Hospital, Takarazuka, Hyogo 665-0827, Japan
[c] Division of Neurology/Molecular Brain Science, Kobe University Graduate School of Medicine, Kobe 650-0017, Japan
[d] Department of Neurology, Aichi Medical University, Aichi 480-1195, Japan

ARTICLE INFO

Article history:
Received 4 May 2014
Received in revised form 3 June 2014
Accepted 3 June 2014
Available online 30 June 2014

Keywords:
Atherosclerosis
Cardiovascular disease
Cholesteryl ester transfer protein deficiency
High density lipoprotein
Hyperalphalipoproteinemia
Stroke

ABSTRACT

Marked hyperalphalipoproteinemia (HAL) is a heterogeneous syndrome. To clarify the pathophysiological significance of HAL, we compared clinical profiles between marked HAL subjects with and without cholesteryl ester transfer protein (CETP) deficiency. CETP deficiency was associated with cardiovascular diseases and strokes in the HAL population, particularly in female. HAL women without CETP deficiency tended to have higher prevalence with cancer history. HAL may not always be a longevity marker, but be sometimes accompanied with pathological conditions.

1. Introduction

Hyperalphalipoproteinemia (HAL) had been regarded as a longevity syndrome. Matsuzawa et al. reported that a man with HAL unexpectedly had a corneal opacity which is a clinical sign for high density lipoprotein (HDL) deficiency [1]. Following studies revealed that genetic deficiency of cholesteryl ester transfer protein (CETP) is a major cause for HAL in Japan [2,3]. CETP is a plasma glycoprotein which facilitates the transfer of cholesteryl ester from HDL to apolipoprotein

* Corresponding author at: Laboratory for Cardiovascular Disease, Novel, Non-invasive, and Nutritional Therapeutics (CNT) and Department of Cardiovascular Medicine, Graduate School of Medicine, Osaka University, 6-2-3, Furuedai, Suita, Osaka 565-0874, Japan. Fax: +81 6 6872 8219.
E-mail addresses: khirano@cnt-osaka.com, khirano@cardiology.med.osaka-u.ac.jp (K. Hirano).
[1] These authors equally contributed to this work.

http://dx.doi.org/10.1016/j.ymgmr.2014.06.001

B-containing lipoproteins, then determine the plasma levels of HDL-cholesterol and low-density lipoprotein (LDL)-cholesterol levels [4]. This protein also regulates the lipid composition and particle size of lipoproteins.

CETP deficiency presents marked HAL and relative decrease in LDL-cholesterol level [5]. Such lipid profiles are generally believed protective for cardiovascular diseases (CVDs) and strokes, however, there has been a controversy whether this genetic deficiency is overall anti- or pro-atherogenic [6–8]. In addition, it is noteworthy that some clinical trials with CETP inhibitors recently failed and terminated [9], suggesting that further understanding pathophysiological significance for HAL is obviously required.

Here, we examined the prevalence of CVDs and strokes in HAL subjects with and without CETP deficiency along with their respective lipid profiles in a specific community, Akita Prefecture, Japan, where we reported that genetic CETP deficiency accumulates [10].

2. Subjects and methods

2.1. Subjects

The surveyed population comprised residents aged over 20-years-old in a community in Daisen City, Akita Prefecture, Japan (http://www.city.daisen.akita.jp/content/docs/english/), which includes Omagari area where genetic CETP deficiency accumulates [9,10].

After the opt-out in the community journal, we directly sent a request letter to 343 people with marked HAL (HDL-C > 100 mg/dL) based upon the annual health examination for the last three years. Unrelated 181 individuals (53%) agreed to participate in this study. Physical examination, blood test, and interview for medical histories and records of CVDs and strokes were performed. Based upon the analyses of the CETP gene and the protein levels, the subjects with HAL were divided into CETP-deficient and non-CETP-deficient groups.

This study was approved by the ethical committee in Osaka University.

2.2. Medical interview

We performed interviews on smoking, alcohol consumption, and medical histories for CVDs, stroke, diabetes mellitus, hypertension, hyperlipidemia, and cancer.

Diagnoses of hypertension and diabetes mellitus were made according to the criteria of Japanese Society of Hypertension and Japan Diabetes Society. CVDs include non-fatal myocardial infarction, angina pectoris, congestive heart failure, and arteriosclerosis obliterans. Strokes include cerebral infarction and cerebral hemorrhage, but exclude subarachnoid hemorrhage and strokes associated with atrial fibrillation. Cancers included any malignant tumors treated previously and currently.

2.3. CETP gene analyses

We performed direct sequencing of the DNA fragments amplified by polymerase chain reaction to detect two common CETP gene mutations [11,12]: intron 14 splicing defect (c.1321 + 1G>A, rs5742907) and missense mutation in exon 15 (c.1376A>G, rs2303790).

2.4. CETP protein mass

CETP protein mass was measured by the commercial available ELISA kit according to the manufacturer's protocol [13,14].

2.5. Criteria for CETP deficiency

Criteria of CETP deficiency was one of the following: 1) either of the common genetic mutations with c.1321 + 1G>A or c.1376A>G. We previously reported that these two CETP gene mutations contributed to approximately 90% of the genetic CETP deficiency in Japan (13, 14); 2) CETP mass was below 2.0 μg/mL.

We decided to use this cut-off value because the mean CETP mass level of the heterozygote for the missense mutation in exon 15 was 1.65 ± 0.31 μg/mL, as reported by Goto et al. [14].

2.6. Lipoproteins analyses

Serum lipoproteins were analyzed by analytical HPLC service system (LipoSEARCH®) at Skylight Biotech Inc. (Akita, Japan), as previously described [15].

2.7. Statistical methods

Data are presented as means (SD). All pair-wise comparisons between CETP- and non-CETP deficient groups were performed with the two-sided Student's *t*-test, and differences in percent values between these two groups were examined by Fisher's exact test. p Values < 0.05 were considered significant.

3. Results

Among the 181 participants with marked HAL, the numbers of CETP-deficient and non-CETP-deficient subjects were 71 and 110, respectively. There were no statistical significance of age and listed coronary risk factors, including hypertension, diabetes mellitus, and cigarette smoking (Table 1).

Among 71 CETP-deficient subjects, 2 were revealed to be homozygous. Prevalence of CVDs history was significantly higher in CETP-deficient group than in non-CETP-deficient group ($p = 0.016$). Particularly in female subgroups, the prevalence of CVDs and strokes was significantly higher in CETP-deficient female ($p = 0.02$ for CVD, $p = 0.028$ for ischemic stroke) (Table 1). Furthermore, the prevalence of cancer history tended to be higher in non-CETP-deficient females than in CETP-deficient ones, although not significant statistically (Table 1). Among HAL women without CETP deficiency, the histories for gastric and uterine/breast cancers seem to be higher.

The particle sizes of HDL and LDL were not different significantly between CETP-deficient and non-CETP-deficient groups. HDL-TG/HDL-cholesterol ratio was significantly decreased in CETP-deficient group than non-CETP-deficient group ($p = 0.002$), whereas LDL-TG/LDL-cholesterol ratio was significantly increased in CETP-deficient group ($p = 0.01$) (Table 1), which is compatible with our previous reports [16,17].

4. Discussion

In the previous cross-sectional study in Omagari area, Japan, where CETP deficiency accumulates, we found that there was a U-shaped relationship between plasma HDL-cholesterol and ischemic electrocardiographic changes for the first time [10]. Zhong et al. reported that heterozygous CETP deficiency may be associated with CVDs in Japanese-American population in Hawaii [18], consistent with results of our previous study. Further, recent reports have drawn U-shaped relationship between plasma HDL-C levels and prevalence of CVDs in the other subjects and population [19,20]. The results of this study, together with those of previous studies, provide evidence that HAL is not always promising for the preventions of CVDs and strokes.

We and others reported that CETP deficiency results in qualitative and quantitative abnormalities in both HDL and LDL [16,17], as shown in Table 1. Triglyceride-rich LDL had lower affinity for LDL receptor [17] and may be susceptible for oxidation in plasma. There seems to be controversial whether large and cholesterol-rich HDL from CETP deficiency had reduced or improved ability for cholesterol efflux from lipid-laden macrophages, depending on their experimental settings [16,21,22].

Unexpectedly, we noticed that the cancer history tended to be more frequent in HAL without CETP deficiency than with CETP deficiency (Table 1). It is known that the Akita Prefecture has one of the highest cancer mortalities among all prefectures in Japan last couple of decades. Further study would be of significance to know the association between HAL and cancer for public health as well as medical science.

The present study has the following limitations: 1) we focused on subjects with marked HAL who voluntarily participated. Therefore, residents with some clinical problems might be more motivated to participate compared with those without any clinical problems, which might raise a possibility that the

Table 1
Clinical profiles in subjects with marked hyperalphalipoproteinemia with and without CETP deficiency.

	CETP deficiency	Non-CETP deficiency	P
Total number	71	110	
Age (y)	67 ± 12	64 ± 13	0.263
CETP mass (mg/mL)	1.7 ± 0.5	2.8 ± 0.5	0.0009
Coronary risk factors			
Hypertension	22 (31%)	36 (33%)	0.878
LDL-cholesterol (mg/dL)	98 ± 24	103 ± 29	0.284
Diabetes mellitus	4 (6%)	10 (9%)	0.572
Smoking habit	18 (26%)	29 (26%)	1.00
Triglycerides:cholesterol ratio in HDL	0.15 ± 0.03	0.21 ± 0.03	0.002
Triglycerides:cholesterol ratio in LDL	0.28 ± 0.04	0.22 ± 0.04	0.01
Cardiovascular disease	10 (14%)	3 (3%)	0.016
Stroke	5 (7%)	4 (4%)	0.487
Ischemic	5 (7%)	3 (3%)	0.271
Hemorrhagic	0 (0%	1 (1%)	1.00
Cancers	8 (11%)	19 (17%)	0.399
Gastric cancer	5 (7%)	10 (9%)	0.786
Male (n)	28	44	
Cardiovascular disease	3 (11%)	2 (5%)	0.386
Stroke	1 (4%)	4 (9%)	0.645
Ischemic	1 (4%)	3 (7%)	1.00
Hemorrhagic	0 (0%)	1 (2%)	1.00
Cancers	5 (18%)	6 (14%)	0.747
Gastric cancer	4 (14%)	5 (14%)	0.734
Others	1 (4%)	1 (4%)	1.00
Female (n)	43	66	
Cardiovascular disease	7 (16%)	1 (2%)	0.02
Stroke	4 (9%)	0 (0%)	0.028
Ischemic	4 (9%)	0 (0%)	0.028
Hemorrhagic	0 (0%)	0 (0%)	1.00
Cancers	3 (7%)	13 (20%)	0.165
Gastric cancer	1 (2%)	5 (8%)	0.404
Uterine, breast cancers	2 (5%)	7 (11%)	0.48
Others	0 (0%)	1 (2%)	1.00

Data are presented as mean ± SD (p value assessed by use of Student's *t*-test) and percentages by Fisher's exact test.
Diagnoses of hypertension and diabetes mellitus were made according to the criteria of the Japanese Society of Hypertension and the Japan Diabetes Society.
Cardiovascular diseases include non-fatal myocardial infarction, angina pectoris, congestive heart failure, and arteriosclerosis obliterans.
Stroke includes cerebral infarction and cerebral hemorrhage, and excludes subarachnoid hemorrhage and strokes associated with atrial fibrillation. Cancers include any malignant tumors treated previously and currently.

disease prevalence might be overestimated in both CETP- and non-CETP deficient HAL groups. It would be of importance to compare the disease prevalence in subjects with marked HAL with that in normolipidemic subjects in the same community; 2) we did not know the molecular basis for HAL without CETP deficiency, although molecules such as hepatic triglyceride lipase [7,22] were reported as responsible for some types of HAL.

In conclusion, marked HAL is not always beneficial for the prevention of CVDs and strokes. Rather, marked HAL may be occasionally associated with the developments of these life-threatening diseases, depending on their sexes and genetic backgrounds.

Acknowledgment

The authors would like to thank Dr. Yoshinobu Ikeda, Dr. Yoshiya Toyoshima, and Professor Mitsuyo Okazaki for their helpful comments and discussion. This study was partially supported by research grant

from rare and intractable disease (H21-Nanchi-Ippan-165) from the Ministry of Health, Labor, and Welfare, Japan.

References

[1] Y. Matsuzawa, S. Yamashita, K. Kameda, M. Kubo, S. Tarui, I. Hara, Marked hyper-HDL2-cholesterolemia associated with premature corneal opacity. A case report, Atherosclerosis 53 (1984) 207–212 (http://www.ncbi.nlm.nih.gov/pubmed/6517975).
[2] J. Koizumi, H. Mabuchi, A. Yoshimura, I. Michishita, M. Takeda, H. Itoh, Y. Sakai, T. Sakai, K. Ueda, R. Takeda, Deficiency of serum cholesteryl-ester transfer activity in patients with familial hyperalphalipoproteinaemia, Atherosclerosis 58 (1985) 175–186 (http://www.ncbi.nlm.nih.gov/pubmed/3937535).
[3] S. Yamashita, Y. Matsuzawa, M. Okazaki, H. Kako, T. Yasugi, H. Akioka, K. Hirano, S. Tarui, Small polydisperse low density lipoproteins in familial hyperalphalipoproteinemia with complete deficiency of cholesteryl ester transfer activity, Atherosclerosis 70 (1988) 7–12 (http://www.ncbi.nlm.nih.gov/pubmed/3355618).
[4] A.R. Tall, Plasma cholesteryl ester transfer protein, J. Lipid Res. 34 (1993) 1255–1274 (http://www.ncbi.nlm.nih.gov/pubmed/8409761).
[5] A. Inazu, M.L. Brown, C.B. Hesler, L.B. Agellon, J. Koizumi, K. Takata, Y. Maruhama, H. Mabuchi, A.R. Tall, Increased high-density lipoprotein levels caused by a common cholesteryl-ester transfer protein gene mutation, N. Engl. J. Med. 323 (1990) 1234–1238, http://dx.doi.org/10.1056/NEJM199011013231803.
[6] C.J. Fielding, R.J. Havel, Cholesteryl ester transfer protein: friend or foe? J. Clin. Invest. 97 (1996) 2687–2688, http://dx.doi.org/10.1172/JCI118719.
[7] K. Hirano, S. Yamashita, Y. Kuga, N. Sakai, S. Nozaki, S. Kihara, T. Arai, K. Yanagi, S. Takami, M. Menju, et al., Atherosclerotic disease in marked hyperalphalipoproteinemia. Combined reduction of cholesteryl ester transfer protein and hepatic triglyceride lipase, Arterioscler. Thromb. Vasc. Biol. 15 (1995) 1849–1856 (http://www.ncbi.nlm.nih.gov/pubmed/7583564).
[8] K. Hirano, S. Yamashita, Y. Matsuzawa, Pros and cons of inhibiting cholesteryl ester transfer protein, Curr. Opin. Lipidol. 11 (2000) 589–596 (http://www.ncbi.nlm.nih.gov/pubmed/11086331).
[9] P.J. Barter, K.A. Rye, Cholesteryl ester transfer protein inhibition as a strategy to reduce cardiovascular risk, J. Lipid Res. 53 (2012) 1755–1766, http://dx.doi.org/10.1194/jlr.R024075.
[10] K. Hirano, S. Yamashita, N. Nakajima, T. Arai, T. Maruyama, Y. Yoshida, M. Ishigami, N. Sakai, K. Kameda-Takemura, Y. Matsuzawa, Genetic cholesteryl ester transfer protein deficiency is extremely frequent in the Omagari area of Japan. Marked hyperalphalipoproteinemia caused by CETP gene mutation is not associated with longevity, Arterioscler. Thromb. Vasc. Biol. 17 (1997) 1053–1059 (http://www.ncbi.nlm.nih.gov/pubmed/9194754).
[11] T. Maruyama, N. Sakai, M. Ishigami, K. Hirano, T. Arai, S. Okada, E. Okuda, A. Ohya, N. Nakajima, K. Kadowaki, E. Fushimi, S. Yamashita, Y. Matsuzawa, Prevalence and phenotypic spectrum of cholesteryl ester transfer protein gene mutations in Japanese hyperalphalipoproteinemia, Atherosclerosis 166 (2003) 177–185 (http://www.ncbi.nlm.nih.gov/pubmed/12482565).
[12] M. Nagano, S. Yamashita, K. Hirano, M. Takano, T. Maruyama, M. Ishihara, Y. Sagehashi, T. Kujiraoka, K. Tanaka, H. Hattori, N. Sakai, N. Nakajima, T. Egashira, Y. Matsuzawa, Molecular mechanisms of cholesteryl ester transfer protein deficiency in Japanese, J. Atheroscler. Thromb. 11 (2004) 110–121 (http://www.ncbi.nlm.nih.gov/pubmed/15256762).
[13] K. Saito, K. Kobori, H. Hashimoto, S. Ito, M. Manabe, S. Yokoyama, Epitope mapping for the anti-rabbit cholesteryl ester transfer protein monoclonal antibody that selectively inhibits triglyceride transfer, J. Lipid Res. 40 (1999) 2013–2021 (http://www.ncbi.nlm.nih.gov/pubmed/10553005).
[14] A. Goto, K. Sasai, S. Suzuki, T. Fukutomi, S. Ito, T. Matsushita, M. Okamoto, T. Suzuki, M. Itoh, K. Okumura-Noji, S. Yokoyama, Cholesteryl ester transfer protein and atherosclerosis in Japanese subjects: a study based on coronary angiography, Atherosclerosis 159 (2001) 153–163 (http://www.ncbi.nlm.nih.gov/pubmed/11689217).
[15] M. Okazaki, S. Usui, A. Fukui, I. Kubota, H. Tomoike, Component analysis of HPLC profiles of unique lipoprotein subclass cholesterols for detection of coronary artery disease, Clin. Chem. 52 (2006) 2049–2053, http://dx.doi.org/10.1373/clinchem.2006.070094.
[16] M. Ishigami, S. Yamashita, N. Sakai, T. Arai, K. Hirano, H. Hiraoka, K. Kameda-Takemura, Y. Matsuzawa, Large and cholesteryl ester-rich high-density lipoproteins in cholesteryl ester transfer protein (CETP) deficiency can not protect macrophages from cholesterol accumulation induced by acetylated low-density lipoproteins, J. Biochem. 116 (1994) 257–262 (http://www.ncbi.nlm.nih.gov/pubmed/7822240).
[17] N. Sakai, S. Yamashita, K. Hirano, M. Ishigami, T. Arai, K. Kobayashi, T. Funahashi, Y. Matsuzawa, Decreased affinity of low density lipoprotein (LDL) particles for LDL receptors in patients with cholesteryl ester transfer protein deficiency, Eur. J. Clin. Invest. 25 (1995) 332–339 (http://www.ncbi.nlm.nih.gov/pubmed/7628520).
[18] S. Zhong, D.S. Sharp, J.S. Grove, C. Bruce, K. Yano, J.D. Curb, A.R. Tall, Increased coronary heart disease in Japanese-American men with mutation in the cholesteryl ester transfer protein gene despite increased HDL levels, J. Clin. Invest. 97 (1996) 2917–2923, http://dx.doi.org/10.1172/JCI118751.
[19] J.P. Corsetti, W. Zareba, A.J. Moss, D.L. Rainwater, C.E. Sparks, Elevated HDL is a risk factor for recurrent coronary events in a subgroup of non-diabetic postinfarction patients with hypercholesterolemia and inflammation, Atherosclerosis 187 (2006) 191–197, http://dx.doi.org/10.1016/j.atherosclerosis.2005.09.012.
[20] T. Costacou, R.W. Evans, T.J. Orchard, High-density lipoprotein cholesterol in diabetes: is higher always better? J. Clin. Lipidol. 5 (2011) 387–394, http://dx.doi.org/10.1016/j.jacl.2011.06.011.
[21] W. Plengpanich, W. Le Goff, S. Poolsuk, Z. Julia, M. Guerin, W. Khovidhunkit, CETP deificiency due to a novel mutation in the CETP gene promoter and its effect on cholesterol efflux and selective uptake into hepatocytes, Atherosclerosis 216 (2011) 370–373, http://dx.doi.org/10.1016/j.atherosclerosis.2011.01.051 (Epub 2011 Feb 26).
[22] P.E. Khoury, W. Plengpanich, E. Frisdal, W. Le Goff, W. Khovidhunkit, M. Guerin, Improved plasma cholesterol efflux capacity from human macrophages in patients with hyperalphalipoproteinemia, Atherosclerosis 234 (2014) 193–199, http://dx.doi.org/10.1016/j.atherosclerosis.2014.02.032 (Epub 2014 Mar 12).

Neurobiology of Disease

The Role of Pak-Interacting Exchange Factor-β Phosphorylation at Serines 340 and 583 by PKCγ in Dopamine Release

Toshihiko Shirafuji,[1] Takehiko Ueyama,[1] Ken-ichi Yoshino,[1] Hideyuki Takahashi,[1] Naoko Adachi,[1] Yukio Ago,[2] Ken Koda,[2] Tetsuaki Nashida,[2] Naoki Hiramatsu,[2] Toshio Matsuda,[2] Tatsushi Toda,[3] Norio Sakai,[4] and Naoaki Saito[1]

[1]Laboratory of Molecular Pharmacology, Biosignal Research Center, Kobe University, Kobe 657-8501, Japan, [2]Laboratory of Medicinal Pharmacology, Graduate School of Pharmaceutical Sciences, Osaka University, Suita, Osaka 565-0871, Japan, [3]Division of Neurology/Molecular Brain Science, Kobe University Graduate School of Medicine, Kobe 650-0017, Japan, and [4]Department of Molecular and Pharmacological Neuroscience, Graduate School of Biomedical Sciences, Hiroshima University, Hiroshima 734-8551, Japan

Protein kinase C (PKC) has been implicated in the control of neurotransmitter release. The AS/AGU rat, which has a nonsense mutation in PKCγ, shows symptoms of parkinsonian syndrome, including dopamine release impairments in the striatum. Here, we found that the AS/AGU rat is PKCγ-knock-out (KO) and that PKCγ-KO mice showed parkinsonian syndrome. However, the PKCγ substrates responsible for the regulated exocytosis of dopamine *in vivo* have not yet been elucidated. To identify the PKCγ substrates involved in dopamine release, we used PKCγ-KO mice and a phosphoproteome analysis. We found 10 candidate phosphoproteins that had decreased phosphorylation levels in the striatum of PKCγ-KO mice. We focused on Pak-interacting exchange factor-β (βPIX), a Cdc42/Rac1 guanine nucleotide exchange factor, and found that PKCγ directly phosphorylates βPIX at Ser583 and indirectly at Ser340 in cells. Furthermore, we found that PKC phosphorylated βPIX *in vivo*. Classical PKC inhibitors and βPIX knock-down (KD) significantly suppressed Ca^{2+}-evoked dopamine release in PC12 cells. Wild-type βPIX, and not the βPIX mutants Ser340 Ala or Ser583 Ala, fully rescued the decreased dopamine release by βPIX KD. Double KD of Cdc42 and Rac1 decreased dopamine release from PC12 cells. These findings indicate that the phosphorylation of βPIX at Ser340 and Ser583 has pivotal roles in Ca^{2+}-evoked dopamine release in the striatum. Therefore, we propose that PKCγ positively modulates dopamine release through β2PIX phosphorylation. The PKCγ-βPIX-Cdc42/Rac1 phosphorylation axis may provide a new therapeutic target for the treatment of parkinsonian syndrome.

Key words: βPIX; Cdc42; dopamine; Parkinson's disease; phosphoproteome; PKC

Introduction

Protein kinase C (PKC) is an important kinase in the enhancement of Ca^{2+}-triggered exocytosis (Iwasaki et al., 2000; Barclay et al., 2003). The PKC family consists of at least 10 subtypes and is divided into the following three subfamilies: conventional PKC (cPKC), novel PKC, and atypical PKC (Nishizuka, 1988, 1992). Among PKCs, only cPKCs (including PKCγ, which is a neuron-specific PKC isoform; Saito and Shirai, 2002) are activated by Ca^{2+} because they contain a C2 domain that specifically binds to Ca^{2+} and phosphatidylserine (PS; Murray and Honig, 2002).

Received Oct. 6, 2013; revised May 18, 2014; accepted May 29, 2014.

Author contributions: N. Saito designed research; T.S., H.T., N.A., Y.A., K.K., T.N., and N.H. performed research; K.Y. contributed unpublished reagents/analytic tools; T.U., T.M., T.T., N. Sakai, and N. Saito analyzed data; T.S., T.U., and N. Saito wrote the paper.

We thank Sumio Sugano (University of Tokyo) and Yoshihide Hayashizaki (RIKEN Omics Science Center and Research Association for Biotechnology) for kindly providing the βPIX cDNA and Hiroshi Kiyonari and Kazuki Nakao (RIKEN CDB) for mice preservation.

The authors declare no competing financial interests.

Correspondence should be addressed to Naoaki Saito, 1-1 Rokkodai-cho, Nada-ku, Kobe 657-8501 Japan. E-mail: naosaito@kobe-u.ac.jp.

DOI:10.1523/JNEUROSCI.4278-13.2014

 0270-6474/14/349268-13$15.00/0

The AS/AGU rat, a spontaneously occurring mutated animal that exhibits locomotor abnormalities, progressive dopaminergic (DAergic) neuronal degeneration in the substantia nigra (SN), and lower extracellular levels of dopamine (DA) in the striatum, has been used as a valuable model for parkinsonian syndrome (Payne et al., 2000). It is noteworthy that a mutation in PKCγ that leads to the early termination at the C2 domain without possessing the catalytic domain causes parkinsonian syndrome in AS/AGU rats (Craig et al., 2001). The mutation in AS/AGU rats should result in the kinase-dead form of PKCγ, but it is still unclear how the mutation causes parkinsonian symptoms.

PKC has been shown to modify exocytosis in at least three steps: (1) increased vesicle recruitment into readily releasable pools (Gillis et al., 1996; Stevens and Sullivan, 1998), (2) acceleration of fusion pore expansion (Scepek et al., 1998), and (3) changes in the kinetics of exocytosis (Graham et al., 2002). However, only the functional consequences of the phosphorylation of SNAP25 (Iwasaki et al., 2000), synaptotagmin I (Hilfiker et al., 1999), and Munc18 (Barclay et al., 2003) by PKC have been established on exocytosis *in vivo*. Furthermore, no attempts have been made to achieve a comprehensive understanding of DA exocytosis through an identification of

PKCγ substrates. Therefore, we attempted to identify the PKC substrates involved in exocytosis to reveal the mechanisms of regulated exocytosis.

Pak-interacting exchange factor-β (βPIX) is a Rho guanine nucleotide exchange factor (GEF) that specifically activates Rac1 and Cdc42 (Shin et al., 2002; Shin et al., 2004; Chahdi et al., 2005; Feng et al., 2006; Shin et al., 2006; ten Klooster et al., 2006; Chahdi and Sorokin, 2008). βPIX has been reported to be an essential element of the exocytotic machinery in neuroendocrine cells (Audebert et al., 2004; Momboisse et al., 2009). To date, there have been several studies on βPIX phosphorylation (Shin et al., 2002; Chahdi et al., 2005; Shin et al., 2006; Mayhew et al., 2007), but there have been no reports of the involvement of βPIX phosphorylation in DA release.

In the present study, we found that the AS/AGU rat is indeed a PKCγ-knock-out (KO) animal, and our phosphoproteome analysis using PKCγ KO mice found 10 candidates in the striatum that are phosphorylated by PKCγ. Among the 10 candidates, we demonstrated that PKCγ activated DA release through the phosphorylation of βPIX.

Materials and Methods

Antibodies. The anti-GFP antibody (Ab) and the anti-vesicular monoamine transporter 2 (VMAT2) Ab recognizing the C-terminal of mouse VMAT2 were prepared in house. The anti-PKCγ (C2-domain) monoclonal Abs specifically recognizing C2-domain of PKCγ have been described previously (Kose et al., 1990). The following Abs were purchased: anti-FLAG from Sigma-Aldrich (catalog #P2983 RRID:AB_439685); anti-βPIX (SH3 domain) from Millipore; anti-β-actin (catalog #ab66338 RRID:AB_2289239) and anti-PKCγ (N-terminal) specifically recognizing N-terminal of PKCγ from Abcam; anti-glutathione S-transferase (GST) (catalog #sc-33613 RRID:AB_647588), anti-PKCα (catalog #sc-208 RRID:AB_2168668), anti-PKCβ1 (catalog #sc-209 RRID:AB_2168968), anti-PKCβ2 (catalog #sc-210 RRID:AB_2252825), and anti-PKCγ (catalog #sc-211 RRID:AB_632234) from Santa Cruz Biotechnology; and anti-serPKC motif (catalog #2261S RRID: AB_330310), anti-βPIX (catalog #4515S RRID:AB_2274365) for immunoprecipitation (IP), and anti-postsynaptic density-95 (PSD95; catalog #2507S RRID:AB_10695259) from Cell Signaling Technology.

Production of anti-phosphoThr76, anti-phosphoSer340, anti-phosphoSer583, and anti-β2PIX Abs. The production of anti-phospho Abs was performed as described previously (Matsubara et al., 2012). For the preparation of anti-phospho-Thr76 (pT76), anti-phospho-Ser340 (pS340), and anti-phospho-Ser583 (pS583) βPIX Abs, oligopeptides corresponding to the amino acids of human βPIX containing pT76 [VSPKSG(pT)LKSPP], pS340 [SASPRM(pS)GFIYQ], and pS583 [SLGRRS(pS)LSRLE] were used as antigens, respectively. After the fifth boost, serum was collected and purified with an affinity column and the non-phospho-antigen peptide. The anti-β2PIX Ab was obtained by eluting the IgG from those that were bound to the nonphospho-Ser583 peptide column.

Animals. The AS/AGU rats were provided by R.W. Davies (Payne et al., 2000). The PKCγ-Cre knockin (KI) mouse was provided by Z.F. Chen (Ding et al., 2005). After the sixth backcross, homozygous littermates obtained by crossing the heterozygous PKCγ-Cre KI mouse were used as the PKCγ KO and wild-type (WT) mice in the studies. All animal studies were approved by the Institutional Animal Care and Use Committee and conducted according to the Kobe University Animal Experimentation Regulations.

Sample preparation and Western blot analysis. The brains from AS/AGU rats and mice were homogenized and the concentrations of the proteins were measured with a bicinchoninic acid (BCA) protein assay kit (Thermo Fisher Scientific). SDS-PAGE and immunoblot analyses were performed as described previously (Adachi et al., 2005).

Preparation of P2 synaptosomal fraction. Adult male mouse brains were collected and homogenized in ice-cold 0.32 M sucrose solution containing 1 mM phenylmethylsulfonyl fluoride, 20 μg/ml leupeptin, and a phosphatase-inhibitor cocktail (Nacalai Tesque). The total homogenate was subjected to centrifugation at 800 × *g* for 12 min at 4°C to remove the nuclei and the supernatant, which we defined as the total fraction, was further centrifuged at high speed at 22,000 × *g* for 20 min at 4°C. The pellet was used as the P2 synaptosomal fraction. To determine the efficiency of the P2 synaptosomal extraction process, we compared the amount of VMAT2 and PSD95 proteins between the total fraction and P2 synaptosomal fraction in the same amount of protein (50 μg), which was calculated using the BCA protein assay kit.

In vivo *microdialysis. In vivo* microdialysis was performed with male mice essentially as described previously (Koda et al., 2010; Ago et al., 2013). In brief, mice were anesthetized by injection of sodium pentobarbital (40 mg/kg, i.p.), and a guide cannula (one site per animal) for a dialysis probe (Eicom) was implanted stereotaxically in the dorsal striatum (anterior 0.1 mm, lateral 1.8 mm, ventral 2.2 mm relative to the bregma and skull; Franklin and Paxinos, 1997). The cannula was cemented in place with dental acrylic and the animals were maintained warm and allowed to recover from anesthesia. The active probe membrane was 1 mm in length. Two days after the surgery, the probe was perfused with Ringer's solution (147.2 mM NaCl, 4.0 mM KCl, and 2.2 mM $CaCl_2$, pH 6.0; Fuso Pharmaceutical Industries) at a constant flow rate of 1 μl/min. To prepare the Ringer's solution containing 100 mM K^+, an identical amount of sodium was replaced for maintaining isoosmolarity. Experiments were initiated after a stabilization period of 3 h. Microdialysis samples (20 μl) were collected every 20 min and were assayed for DA by high-performance liquid chromatography (HPLC) with electrochemical detection. No-net-flux microdialysis experiments were conducted in a PKCγ KO and WT mice as described previously (Justice, 1993; Chefer et al., 2005; Hewett et al., 2010). Three different concentrations of DA in Ringer's solution (C_{in} of 0, 5 and 20 nM DA) were perfused through the probe and DA in the perfusates (C_{out}) was measured in the fifth fraction following 4 fractions (equilibration period) at each applied DA concentration. A slope was calculated for the linear regression for DA applied (C_{in}) and the difference between dopamine applied and DA measured ($C_{in} - C_{out}$). The slope (extraction fraction) is an indirect measure of dopamine transporter (DAT) dynamics *in vivo* to remove extracellular DA.

Measurement of DA and DA metabolite levels in striatum. The concentrations of DA were quantified by HPLC with an electrochemical detector (ECD-100; Eicom; Kawasaki et al., 2006; Kawasaki et al., 2007). Tissue samples were homogenized in 0.2 M perchloric acid containing 100 μM EDTA and isoproterenol as an internal standard. The homogenate was centrifuged at 15,000 × *g* for 15 min at 0°C. The supernatant was filtered through a 0.22 μm membrane filter (Millipore), and then a 10 μl aliquot of the sample was injected onto the HPLC column every 30 min for the DA assay. An Eicompak SC-5ODS column (3.0 mm i.d. × 150 mm; Eicom) was used, and the potential of the graphite electrode (Eicom) was set to +750 mV against an Ag/AgCl reference electrode. The mobile phase contained 0.1 M sodium acetate/0.1 M citrate buffer, pH 3.5, 190 mg/L octanesulfonic acid, 5 mg/L EDTA, and 17% (v/v) methanol. Data were calculated by analyzing the peak area of the external standard of dopamine hydrochloride (Sigma-Aldrich).

Cell culture. COS7 and HEK293 cells were cultured in DMEM and Eagle's minimum essential medium (Nacalai Tesque), respectively, which were supplemented with 10% fetal bovine serum, penicillin (100 units/ml), and streptomycin (100 μg/ml). Nonessential amino acids (100 μM) were added for HEK293 cells. PC12 cells were cultured in DMEM containing 10% fetal bovine serum and 5% horse serum. All cells were cultured at 37°C in a humidified atmosphere containing 5% CO_2.

Construction of plasmids. WT PKCγ was cloned into pcDNA3.1 (Life Technologies) and the subdomains of PKCγ were cloned into pcDNA3.1 with GFP, as described previously (Seki et al., 2005). Human βPIX was provided by the RIKEN BioResource Center through the National BioResource Project of MEXT in Ibaraki, Japan (Ota et al., 2004). For the construction of plasmids encoding full-length β2PIX that was fused with 3xFLAG at the N terminal, β2PIX with a NotI/BamHI site that was produced by PCR was cloned into a 3xpFLAG-CMV10 vector (Sigma-Aldrich). Because the target sequence for rat βPIX knock-down (KD; sh369) was located in the coding region of βPIX, sh369-resistant β2PIX in the 3xpFLAG-CMV10 vector was made by placing 6-base silent

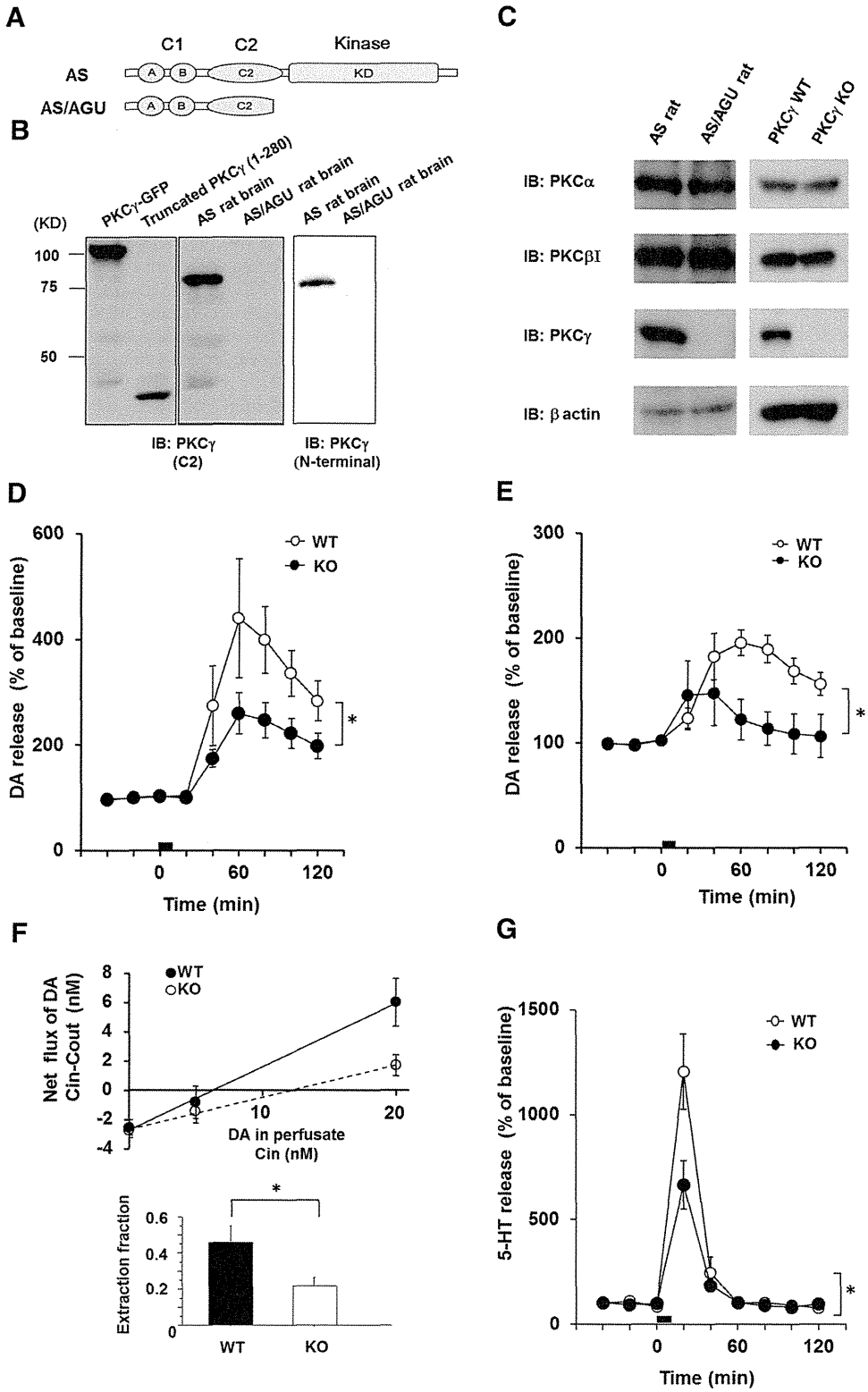

Figure 1. The PKCγ KO model exhibits symptoms of parkinsonian syndrome. ***A***, Schematic illustrations of the PKCγ protein and AS/AGU mutations. The truncated PKCγ polypeptide terminates within the C2 domain. ***B***, Recombinant truncated PKCγ (1–280 aa), which was transfected in COS-7 cells, the AS rat brain lysate, and the AS/AGU rat brain lysate, was detected by immunoblot analysis with an anti-PKCγ (C2-domain) monoclonal antibody and anti-PKCγ (N terminal) antibody, respectively. ***C***, The PKCγ KO was confirmed by immunoblot analysis of the whole brain of the AS/AGU rats and PKCγ KO mice. Arrowheads are recombinant PKCγ-GFP and PKCγ (1–280aa)-GFP, which were used as positive controls. ***D***, *In vivo* microdialysis in the striatum of the PKCγ KO mice. A high level of K^+ was perfused into the striatum through a dialysis probe for the time indicated by the square at 3–4 months. The results are expressed as mean ± SEM ($n = 4–5$, interaction of the genotype and time for DA release that was stimulated by high K^+ levels; $^*p < 0.05$, $F_{(8,48)} = 2.31$, repeated two-way ANOVA). ***E***, *In vivo* microdialysis for DA in the striatum of the PKCγ-KO (KO) mice that were stimulated with METH. METH (1 mg/kg) was perfused into the striatum through a dialysis probe for the time indicated by the square at 3 months (*Figure legend continues.*)

changes within the targeting sequence (5′-CAaACgAGtGAaAAaTTa-3′) with a QuikChange Multisite-Directed Mutagenesis Kit (Agilent Technologies). For construction of plasmids encoding full-length β2PIX or fragments that were fused to GST, full-length β2PIX and the SH3 (1–92 aa), DH (93–274 aa), and PH (275–400 aa) C-terminal (401–625 aa) regions were amplified by PCR with a Not1/BamH1 site and cloned into the pGEX-6P1 vector. Substitutions of Ser or Thr to Ala or Glu at the identified phosphorylation sites (Thr76Ala, Ser215Ala, Ser340Ala or Glu, and Ser583Ala or Glu) were introduced with a QuikChange kit.

Protein expression. Protein expression was performed as described previously (Kawasaki et al., 2010). In brief, BL21 pLys *Escherichia coli* and Sf9 cells were transformed with expression plasmids. *E. coli* and Sf9 cells were harvested and lysed. For the purification of recombinant proteins, GST-fusion proteins were purified with glutathione-Sepharose 4B resin (GE Healthcare Biosciences).

RNAi: short hairpin RNA and small interfering RNA. Double-stranded oligonucleotides were cloned into the short hairpin RNA (shRNA) expression vector, pSuper (puro; Oligoengine). The target sequence for the shRNA rat βPIX KD was 5′-GCAGACCAGCGAGAAGTTGAG-3′ (sh369; cording nucleotides 369–389). Because the βPIX shRNA sequence that we used was common to both the β1 and β2 isoforms, KDs of both β1 and β2 in PC12 cells were examined with βPIX SH3- and β2-specific antibodies. The synthesized small interfering RNA (siRNA) for rat βPIX was composed of a mixture of 4 oligonucleotides (si878: 5′-GGGAUGACAUAAAGACGUU-3′, si806: 5′-AGUGUCAAGAAGU ACGAAA-3′, si1115: 5′-GGAGCAUGAUCGAGCGCAU-3′, and si1153: 5′-CAACAGGACUUGCACGAAU-3′) was purchased from Thermo Fisher Scientific (SmartPool). Verified shRNA plasmids for KD of Cdc42 (sh197; 5′-GATTACGACCGCTGAGTTA-3′; Ueyama et al., 2014) and Rac1 (sh618; 5′-CCTTTGTACGCTTTGCTCA-3′; Ueyama et al., 2006) were described previously.

In vitro *PKC phosphorylation assay.* An *in vitro* PKC phosphorylation assay was performed as described previously (Kawasaki et al., 2010). In brief, precipitated FLAG-tagged β2PIX proteins or purified GST-tagged β2PIX were incubated with 200 ng of GST-tagged PKCγ or GST and the following buffers: 20 mM Tris, pH 7.4, 0.5 mM $CaCl_2$, 10 μM ATP, 0.5 mCi [γ-^{32}P] ATP, 8 μg/ml PS, and 0.8 μg/ml (±)-1,2-didecanoylglycerol (DO) in a 50 μl final volume. The samples were incubated with or without PKC inhibitors, including GF109203X (GFX), which was used as a pan PKC inhibitor, and Gö6976, which was used as a cPKC inhibitor, at 30°C for 15 min. For the calculation of the relative phosphorylation levels, the densitometries of the autoradiography were normalized with the total protein levels. The average relative phosphorylation levels of PKCγ stimulation were defined as 1.00.

PKC phosphorylation assay in cells. A PKC phosphorylation assay in cells was performed as described previously (Kawasaki et al., 2010) but with slight modifications. In brief, HEK293 cells were transfected with WT β2PIX in 3xpFLAG-CMV10 with a NEPA21 electroporator (Nepa Gene). After 12-O-tetradecanoylphorbol 13-acetate (TPA) stimulation with or without PKC inhibitors for 30 min in HEPES buffer at 37°C, the cells were collected and resuspended in homogenization buffer containing 150 mM NaCl, 10 mM ethylene glycol tetraacetic acid, 2 mM ethylenediamine tetracetic acid, 10 mM HEPES, pH 7.4, 1 mM phenylmethylsulfonyl fluoride, 20 μg/ml leupeptin, and a phosphatase-inhibitor cocktail. The precipitated proteins were separated by SDS-PAGE. The phosphorylated proteins were visualized with phospho-Abs. For the calculation of the relative phosphorylation levels, the densitometries of the immunoblots of the phospho-Abs were normalized to the total protein levels in each experiment and the averages of the relative levels of phosphorylation in more than three independent experiments are presented. The phosphorylation levels of the prestimulations were defined as 1.00.

PKC phosphorylation assay in vivo. The mice P2 synaptosomal fraction was resuspended in HEPES buffer containing 1 mM phenylmethylsulfonyl fluoride, 20 μg/ml leupeptin, and a phosphatase-inhibitor mixture and used for the *in vivo* PKC phosphorylation assay (Wu et al., 1982). After 2 μM TPA stimulation with or without 2 μM GFX for 30 min in HEPES buffer at 37°C, the P2 fraction was collected and resuspended in homogenization buffer containing 150 mM NaCl, 10 mM ethylene glycol tetraacetic acid, 2 mM ethylenediamine tetracetic acid, 10 mM HEPES, pH 7.4, 1 mM phenylmethylsulfonyl fluoride, 20 μg/ml leupeptin, and the phosphatase-inhibitor mixture. The precipitated proteins were separated by SDS-PAGE. The phosphorylated proteins were visualized with ser-PKC motif Abs.

DA release assay. DA release assays in βPIX KD cells were performed 96 h after transfection by NEPA21. PC12 cells were washed thrice with 500 μl of incubation solution (140 mM NaCl, 5 mM KCl, 2 mM $CaCl_2$, 1 mM $MgCl_2$, 2 mM glucose, 20 μM pargyline, and 10 mM HEPES, pH 7.5) and then incubated for 60 min in 500 μl of incubation solution with ^{3}H-DA (PerkinElmer), followed by three washes with 500 μl of incubation solution. The cells were allowed to rest or were stimulated with 500 μl of a high-K^+ solution containing 100 mM KCl and 35 mM NaCl for 10 min. The supernatant was collected and the cells were harvested in 500 μl of incubation solution with 2% Triton X-100. The amount of DA that was secreted into the medium and retained in the cells was measured in 500 μl of samples with a scintillation counter LS-6500 (Beckman Coulter). DA secretion was expressed by the following formula: %DA = (^{3}H in supernatant)/(^{3}H in supernatant + ^{3}H in cell lysate). A collagen-IV-coated six-well plate (BD Biosciences) was used for the DA release assay.

Mass spectrometry for β2PIX-phosphorylation site identification. Mass spectrometry for β2PIX-phosphorylation site identification was performed as described previously (Sakuma et al., 2012). After the *in vitro* PKC phosphorylation assay and electrophoresis, silver-stained bands that corresponded to GST-tagged β2PIX proteins were excised and destained. After reduction-alkylation reactions, the proteins in the gels were digested with porcine trypsin (sequencing grade; Promega) in 50 mM ammonium bicarbonate for 15 h at 37°C. The peptide fragments extracted from the gels were subjected to liquid chromatography/tandem mass spectrometry (LC/MS/MS) with a high-performance liquid chromatography system (Paradigm MS4; Michrom Bioresources) coupled to a linear ion trap mass spectrometer (Finnigan LTQ Orbitrap XL; Thermo Fisher Scientific). The LC/MS/MS data were interpreted with a MASCOT MS/MS ions search (Matrix Science).

Phosphoproteome analysis. Phosphoproteome analysis was performed as described previously with some modifications (Saito et al., 2006). Mice striata were dissolved in 50 mM Tris HCl, pH 9.0, 8 M urea, 10 mM ethylenediamine tetracetic acid, 1 mM phenylmethylsulfonyl fluoride, 20 μg/ml leupeptin, and a phosphatase inhibitor mixture. After homogenization with a Dounce homogenizer (10 strokes), the resultant solution was centrifuged at 2000 × *g* for 5 min and the supernatant was collected. The protein amounts were measured with a BCA protein assay kit. The proteins from the striatum were dried and resuspended in 50 mM Tris HCl buffer, pH 9.0, containing 8 M urea at a concentration of 10 μg/μl. These mixtures were subsequently reduced with dithiothreitol, alkylated with acrylamide, and digested with Lys-C endopeptidase at 37°C overnight, followed by trypsin digestion at 37°C overnight. The digested solutions were desalted and concentrated with Empore high-performance extraction disk cartridges (3M). Phosphopeptide enrichment was performed with hydroxy acid-modified metal oxide chromatography (HAMMOC; Titansphere Phos-TiO Kit; GL Sciences; Kyono et al., 2008). For elution of the phosphopeptides, 50 μl of 5% NH_3 and 5% pyrrolidine were used. The fractions were immediately acidified and desalted with SPE-C tips (GL Sciences). A Tomy CC-105 vacuum evap-

←

(Figure legend continued.) ($n = 4$, interaction of the genotype and time for DA release stimulated by METH, $F_{(8,48)} = 3.37$; $^*p < 0.01$, repeated two-way ANOVA). ***F***, No-net flux microdialysis to quantitate basal DAT activity in PKCγ KO mice. Three different concentrations of DA in CSF (0, 5, and 20 nM DA) were perfused through the probes to determine the extracellular DA concentration and extraction fraction. Linear regression for the DA perfused and DA measured provided extraction fraction (slope) as an indirect measure of DAT activity *in vivo* to remove extracellular DA. Extraction fraction for WT and KO mice are shown. Data represent mean ± SEM ($n = 4$ and 5 for WT and KO mice, respectively, $^*p < 0.05$). ***G***, *In vivo* microdialysis of serotonin in the striatum of the PKCγ-KO mice that were stimulated by high K^+ levels. K^+ (100 mM) was perfused into the striatum through a dialysis probe for the time indicated by the square at 3–4 months. The results are expressed as mean ± SEM ($n = 4$, interaction of the genotype and time for serotonin release that was stimulated by high K^+ levels, $F_{(8,48)} = 5.399$; $^*p < 0.001$, repeated two-way ANOVA).

Table 1. DA and DA metabolite levels in the striatum of PKCγ WT and KO mice

Age (mo)	Genotype	DA (ng/g weight)	DOPAC (ng/g weight)	HVA (ng/g weight)
3	KO	19629.5 ± 625.4	1838.6 ± 68.9	1490.6 ± 89.0
	WT	19516.4 ± 361.1	1999.1 ± 103.4	1652.1 ± 18.4
6	KO	20667.2 ± 803.5	1671.2 ± 113.0	1620.0 ± 93.9
	WT	17416.8 ± 781.3	1559.2 ± 77.2	1334.6 ± 63.7
12	KO	28911.0 ± 1801.4	2576.0 ± 277.9	2378.1 ± 161.3
	WT	29564.9 ± 2581.4	2253.1 ± 202.2	2392.2 ± 128.4

Results are expressed as mean ± SEM of 4–5 mice.

HVA, Homovanillic acid.

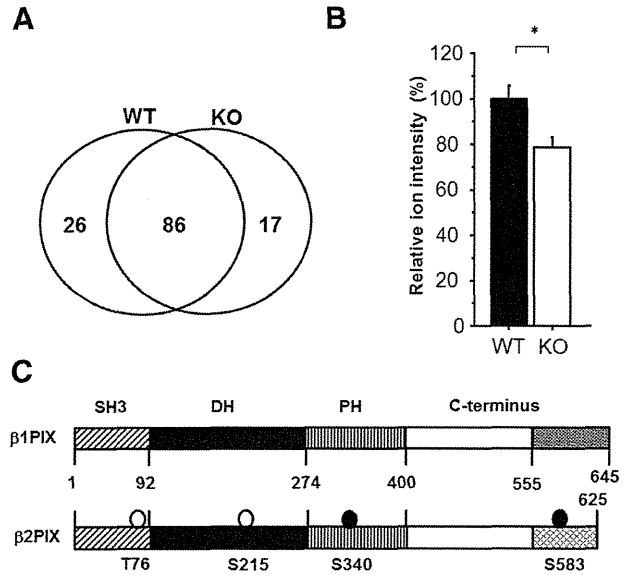

Figure 2. Phosphoproteome analysis revealed 10 phosphopeptides with decreased average ion intensity in PKCγ KO mice striatum. ***A***, Overview of the phosphoproteome (WT, $n = 5$; KO, $n = 4$). ***B***, Average ion intensity of the Ser340 βPIX phosphopeptide is calculated in both PKCγ KO and WT mice ($n = 4–5$; $^*p < 0.05$, unpaired t test). The relative average ion intensity of WT mice was defined as 100%. The results are expressed as mean ± SEM. ***C***, Schematic illustrations of the β1 and β2 PIX protein. The phosphorylation sites that were determined by the *in vitro* PKC phosphorylation assay and the phosphoproteome analysis are circled. The open circles are the phosphorylation sites that were determined only *in vitro*. The closed circles are the phosphorylation sites that were determined *in vitro* and *in vivo*.

orator was used to concentrate the sample and the phosphopeptides were analyzed by LC/MS/MS.

Statistical analysis. The data are presented as mean ± SEM and were analyzed with unpaired t tests, one-way ANOVA with a *post hoc* Dunnett's test, or a repeated two-way ANOVA. The statistical analyses were performed with the Statview 5.0J software package (SAS Institute). p-values of 5% or less were considered statistically significant.

Results

PKCγ KO animals exhibited parkinsonian symptoms, including DA release impairment in the striatum

AS/AGU rats show altered behaviors (Craig et al., 2001), DA release impairment, and the pathology of the nigrostriatal system resembles the pathology observed in human patients with parkinsonian syndrome (Campbell et al., 1996; Payne et al., 2000). AS/AGU rats have a spontaneously occurring mutation that changes the CAG (Glu281) codon to a TAG (stop codon) in PKCγ, and the putatively truncated PKCγ, if produced, will terminate at the fifth residue from the C terminus of the last strand of the β-sheet structure of the C2 domain (Fig. 1*A*). The truncated protein may result in a severe or complete loss of the kinase function of PKCγ, although it has not yet been clarified whether the truncated protein is expressed in AS/AGU rats. Although both anti-PKCγ (N terminal) Ab and anti-PKCγ (C2-domain) Ab detected an 80 kDa single band in AS rats, no band was detected in the AS/AGU rats (Fig. 1*B*). These findings indicated that PKCγ was not expressed in AS/AGU rats, suggesting the hypothesis that PKCγ KO mice show similar symptoms as those observed in AS/AGU rats. We first confirmed that our PKCγ KO mice did not express PKCγ, whereas the expression levels of other members of cPKCs were unaltered (Fig. 1*C*). To determine the effects of the PKCγ KO on DA release in the striatum, we performed *in vivo* microdialysis in the striatum. The basal line extracellular levels of DA in the striatum did not differ significantly between the PKCγ WT and KO mice. After treatment with high levels of K^+ (Fig. 1*D*) and methamphetamine (METH; Fig. 1*E*), the increase in DA release in the WT was significantly larger than that in the KO 3–4 months after birth. Although high K^+ levels induced DA release is mediated by exocytosis and not by DAT, PKC induces DAT endocytosis (Daniels and Amara, 1999), which may decrease the extracellular DA levels by increasing

Table 2. List of phosphopeptides with a PKC phosphorylation motif

Protein name	Accession no.	Sequence	Site	No. of phosphopeptides		Lowest peptide score		Highest peptide score		Average ion intensity		
				WT	KO	WT	KO	WT	KO	WT	KO	WT/KO
Gap junction alpha-1 protein	NP 034418	KVAAGHELQPLAIVDQRPSSRA	S365	7	0	11	—	28	—	3	0.4	7.3
Disks large-associated protein 1	NP 808307	RSLDSLDPAGLLTSPKF	S437	5	0	48	—	77	—	3.4	0.8	4.4
MAP kinase-activating death domain protein	NP 001171190	RATLSDSEIETNSATSAIFGKA	T1235	8	4	40	26	90	58	3.7	1	3.9
DnaJ homolog subfamily C member 5	NP 001258513	RSLSTSGESLYHVLGLDKN	S10	54	55	3	4	88	85	969	299.5	3.2
Calnexin	NP 001103969	KAEEDEILNRSPRN	S582	6	2	25	22	31	34	3.1	1.8	1.8
Stathmin	NP 062615	KRASGQAFELILSPRS	S16	26	23	8	6	93	84	12.1	7.5	1.6
Stathmin	NP 062615	RASGQAFELILSPRS	S25	25	17	5	19	81	83	7.4	5.9	1.3
Rho guanine nucleotide exchange factor 7	NP 001106989	RMSGFIYQGKL	S340	3	0	24	—	59	—	1.8	1.4	1.4
Reticulon-4	NP 077188	RRGSGSVDETLFALPAASEPVIPSSAEKI	S165	15	8	34	41	70	59	2.3	1.7	1.3
α-adducin	NP 001019629	KFRTPSFLKK	S724	3	2	7	9	29	25	6.1	4.8	1.3
β-adducin	NP 001258786	KDIATEKPGSPVKS	S594	10	8	10	17	50	56	0.4	0.3	1.2

Phosphopeptides with a WT/KO ratio >1.0 are listed. The numbers of phosphorylation sites are based on the results of mice in PhosphoSitePlus (www.phosphosite.org). S and T are the identified phosphorylation sites. Number of phosphopeptides means the total numbers of the phosphopeptides in each group ($n = 4$). Highest or lowest peptide score means the highest or lowest peptide score in each group ($n = 4$). Peptides that were not detected are shown as —.

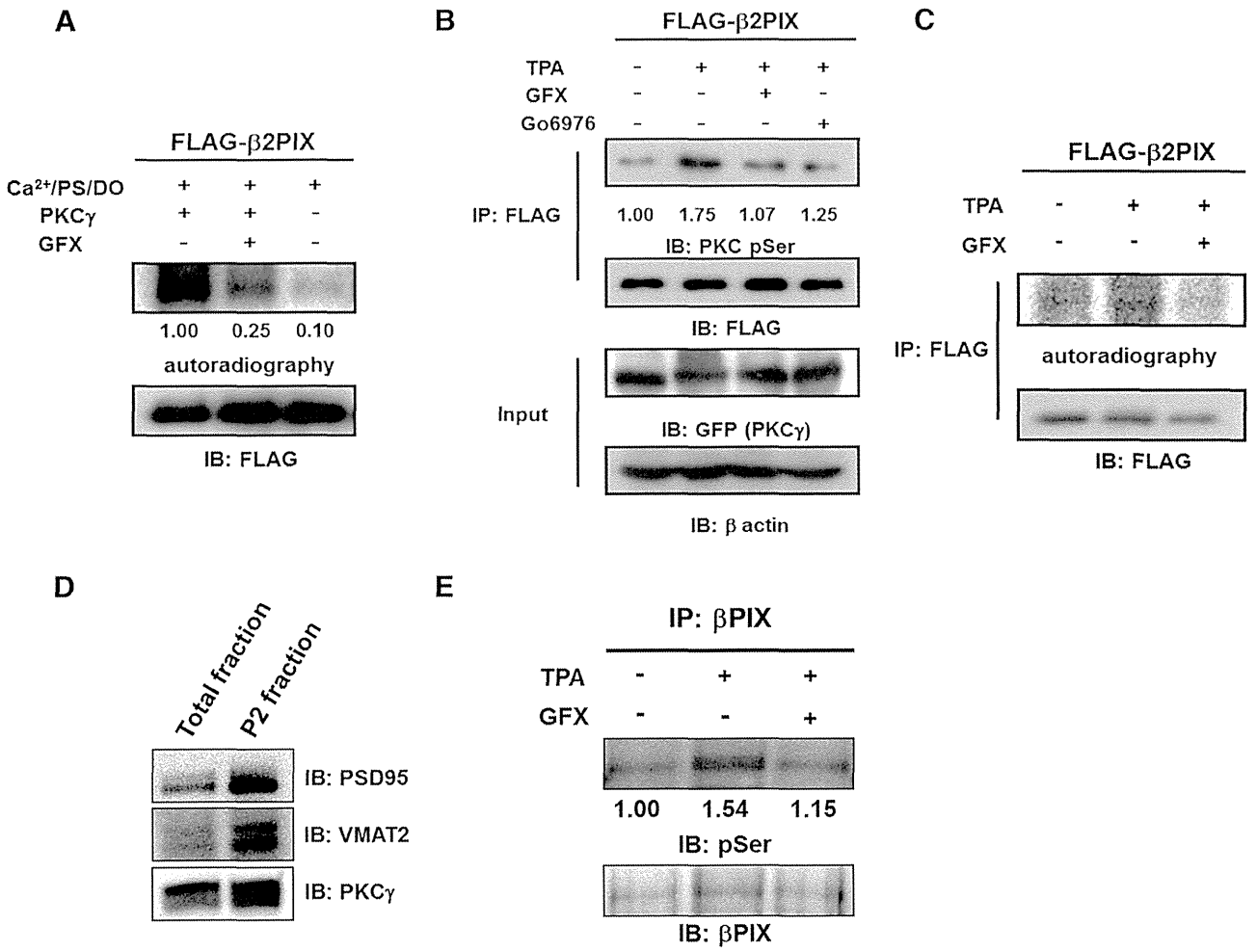

Figure 3. βPIX is phosphorylated by PKCγ *in vitro*, in cells, and *in vivo*. ***A***, *In vitro* phosphorylation of β2PIX. FLAG-tagged β2PIX proteins were purified and incubated with or without recombinant PKCγ in the presence of PKC activator (PS/DO/Ca^{2+}) and [γ-^{32}P] ATP for 20 min. The *in vitro* phosphorylation of β2PIX was also performed in the presence of GFX. The phosphorylated proteins were detected by autoradiography and the levels of protein expression were determined by Western blotting with an anti-FLAG antibody. The numbers show the relative phosphorylation levels that were normalized to PKCγ stimulation as 1.00 ($n = 3$). ***B***, In-cell phosphorylation of β2PIX. HEK293 cells expressing FLAG-tagged β2PIX and GFP-tagged PKCγ were stimulated with 1 μM 12-O-TPA for 20 min in the presence or absence of 1 μM GFX or 1 μM Gö6976. FLAG-tagged β2PIX proteins were purified with anti-FLAG agarose resin. Phosphorylated proteins were detected by an immunoblot analysis with an anti-pSer PKC motif antibody. Protein expression was determined by Western blotting with an anti-FLAG antibody. The average relative phosphorylation levels for each experimental condition were normalized to the prestimulation signal set as 1.00 ($n = 5$). ***C***, PC12 cells expressing FLAG-tagged β2PIX were incubated with ^{32}P monosodium phosphate and stimulated with 1 μM 12-O-TPA in the absence or presence of 1 μM GFX. FLAG-tagged β2PIX proteins were purified with anti-FLAG agarose resin. Phosphorylated proteins were detected by autoradiography, and protein expression was determined by immunoblots with an anti-FLAG antibody. ***D***, The same amount of samples of total fraction and the P2 synaptosomal fraction were immunoblotted by anti-PSD95 antibody as a postsynaptic marker, anti-VMAT2 antibody as a presynaptic marker, and anti-PKCγ antibody. ***E***, the P2 synaptosomal fraction was stimulated with 2 μM 12-O-TPA in the absence or presence of 2 μM GFX. βPIX proteins were purified with anti-βPIX antibody. Phosphorylated proteins were detected by phospho-Abs. The numbers show the relative phosphorylation levels that were normalized to pretreatment as 1.00 ($n = 3$).

DAT activity in PKCγ KO mice striatum. To evaluate the DAT activity in PKCγ KO mice, we performed the no-net-flux microdialysis experiment. The slope (extraction fraction) is the measure of the activity of DAT *in vivo*. Fig. 1*G* shows decreased DAT activity in the striatum of PKCγ KO mice, suggesting that PKCγ KO mice tend to have increased rather than decreased extracellular DA levels compared with WT mice (Fig. 1*F*). Consistent with our results, the increase in the serotonin release stimulated by high K^+ levels in WT was also significantly larger than that of the KO (Fig. 1*G*), as described previously in AS/AGU rats (Al-Fayez et al., 2005). Because we had preliminary data that suggested slight loss of DAergic neurons in 12-month-old, but not 3- or 6-month-old, PKCγ KO mice, there was a possibility that the decrease in DA release in PKCγ KO mice was due to the decrease in DA in the striatum. We measured DA and its metabolites using HPLC in the striatum. No difference in DA or DA metabolite levels in the striatum was observed between PKCγ KO mice and WT mice at 3, 6, and 12 months (Table 1), suggesting that DA release disorder was from the exocytotic machinery disorder instead of the lack of the DAergic neurons in the nigrostriatum system. These results suggested that the PKCγ KO mice would show similar parkinsonian symptoms as those observed in the AS/AGU rats. From the analysis of the PKCγ KO mice and AS/AGU rats, we concluded that PKCγ KO animals could be used as a practical model of parkinsonian syndrome.

Phosphoproteome analysis identified 10 phosphoproteins, including βPIX, with a PKC-phosphorylation motif

We hypothesized that a loss or decrease of PKCγ-mediated phosphorylation in the nigrostriatal system results in DA release im-

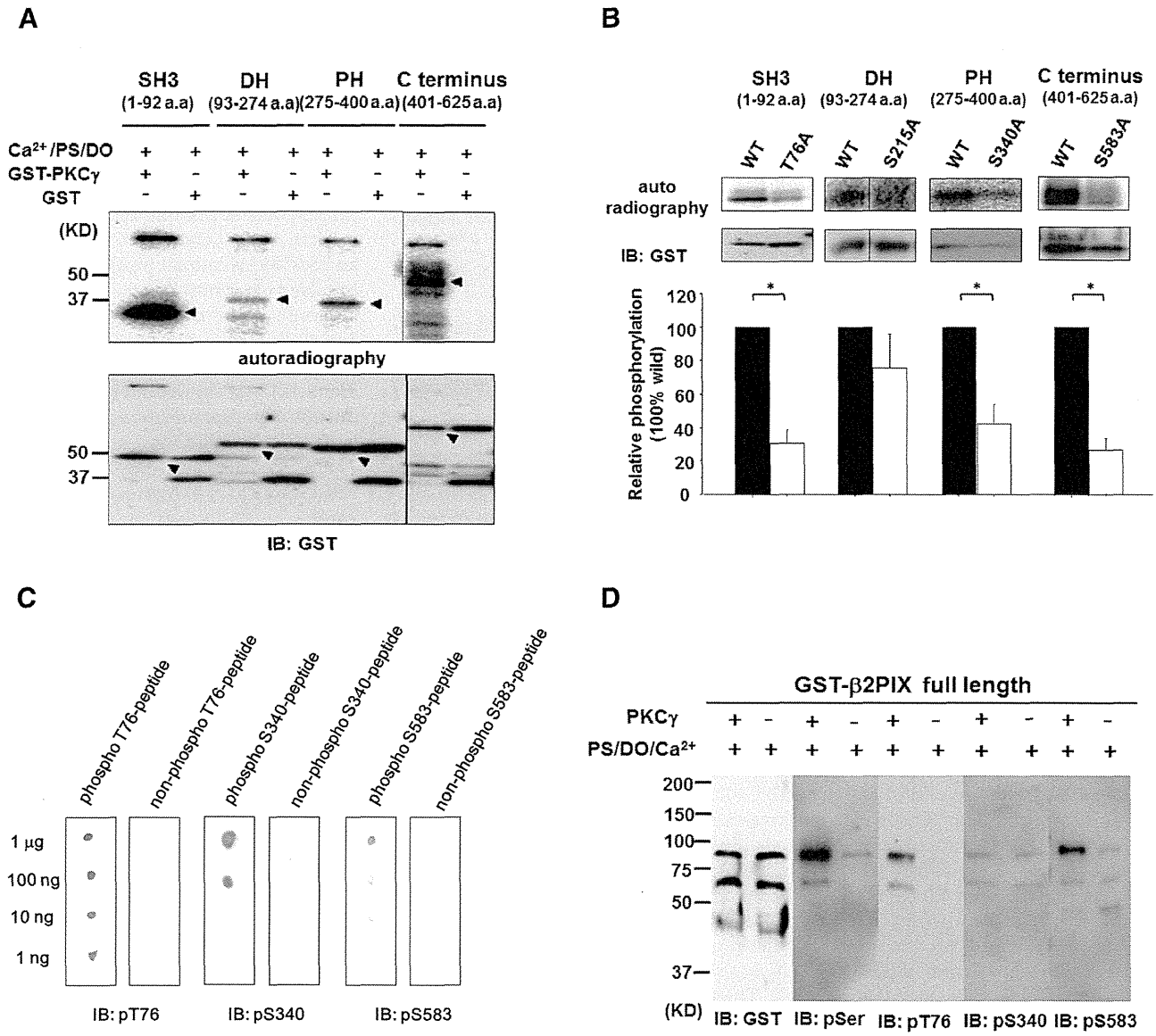

Figure 4. Analysis of the *in vitro* PKCγ phosphorylation sites in β2PIX. ***A***, *In vitro* phosphorylation of the GST-tagged β2PIX SH3, DH, PH, and C terminus regions. Each protein region was expressed in *E. coli*, purified, and incubated with [γ^{32}P] ATP and recombinant PKCγ in the presence of Ca^{2+}, PS, and DO. The phosphorylated proteins were separated by SDS-PAGE and detected by autoradiography (top). The protein levels of the recombinant β2PIX protein regions were detected by Western blotting (bottom). The arrowheads on the top indicate the autoradiography and those on the bottom indicate the total protein for each domain. ***B***, *In vitro* phosphorylation of the β2PIX SH3, DH, PH, and β2 C terminus regions containing the indicated mutations determined by an *in vitro* phosphorylation assay that was followed by mass spectrometry and phosphoproteome analysis. Phosphorylation levels were normalized to the WT phosphorylation signal for each domain, which were set to 100%: SH3 ($n = 5$), DH ($n = 4$), PH ($n = 5$), β2 C terminus ($n = 3$); The results are expressed as mean ± SEM (*$p < 0.05$, unpaired *t* test). ***C***, Specificity of anti-phospho-Thr76, Ser340, and Ser583 antibodies. The indicated amount of the phospho-peptide (pT76 [VSPKSG(pT)LKSPP], pS340 [SASPRM-(pS)GFIYQ], and pS583 [SLGRRS(pS)LSRLE]) or non-phosphopeptide was dotted on the PVDF membrane. Immunostaining was performed using purified anti-pT76, pS340, and pS583 antibodies. ***D***, *In vitro* phosphorylation assay of full-length β2PIX. GST-tagged full-length β2PIX was expressed in *E. coli*, purified, and incubated with ATP and recombinant PKCγ in the presence of Ca^{2+}, PS, and DO. Phosphorylated proteins were separated by SDS-PAGE and detected by an anti-pSer PKC motif antibody, an anti-pT76 antibody, an anti-pS340 antibody, or an anti-pS583 antibody, respectively.

pairment. To identify the substrates for PKCγ, we performed a phosphoproteome analysis using HAMMOC methods (Kyono et al., 2008; Fig. 2*A*). Among the phosphopeptides in the WT group, we chose the proteins that may have a relationship to exocytosis and then calculated the WT/KO ratio of the average ion intensity. The average ion intensity ratio of the phosphopeptides that included the PKC phosphorylation motif are shown in Table 2. Among these 10 candidates, we focused on βPIX (Fig. 2*B*), even when the degree of the phosphorylation decrease was small, because it is expressed in DAergic neurons in the SNpc (http://www.informatics.jax.org/assay/MGI:4944920) and has been reported to play important roles in the machinery of exocytosis (Audebert et al., 2004; Momboisse et al., 2009). In the present phosphoproteome analysis, phosphorylation of Ser340 in β2PIX was detected. The βPIX family consists of two splicing forms, β1 and β2; the difference between β1 and β2 PIX exists in the C terminus (Fig. 2*C*). Although both β1 and β2 contain Ser340, β2PIX is the predominant form in the CNS (Koh et al., 2001). Therefore, β2PIX was used in the present study.

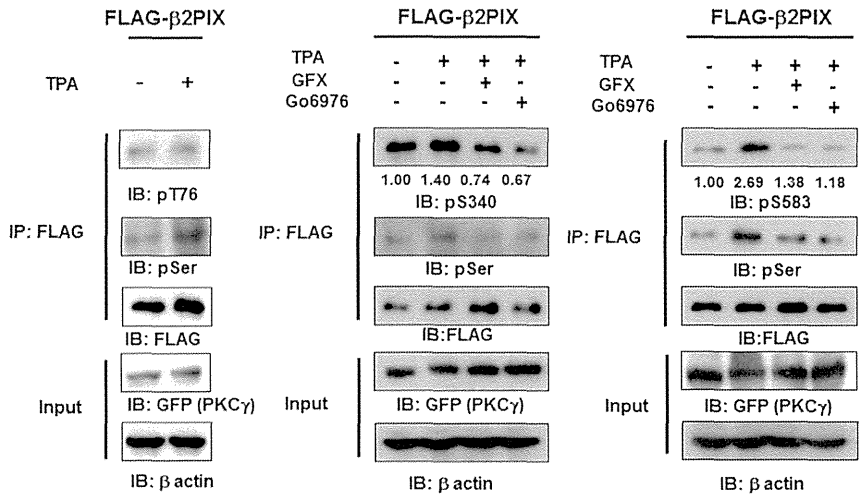

Figure 5. PKC mediates the phosphorylation of full-length β2PIX at Ser340 and Ser583 in cells. HEK293 cells transfected with FLAG-tagged WT β2PIX and GFP-tagged PKCγ were stimulated with 1 μM TPA in the presence or absence of 1 μM GFX, which is a pan-PKC inhibitor, or Gö6976, which is a cPKC inhibitor. FLAG-tagged β2PIX was precipitated and separated by SDS-PAGE. The total amounts of protein were determined by immunoblot analyses with an anti-FLAG antibody. GFP-tagged PKCγ or β actin was detected by anti-GFP or anti-β-actin antibodies. The phosphorylation levels of the FLAG-tagged β2PIX proteins that were determined with an anti-pT76 antibody (***A***; $n = 2$), an anti-pS340 (***B***; $n = 4$), or an anti-pS583 (***C***; $n = 4$) antibody were normalized to the phosphorylation levels of the WT. The numbers show the average relative phosphorylation levels that were normalized to prestimulation levels set as 1.00.

βPIX is phosphorylated by PKCγ *in vitro*, in cells, and *in vivo*

To determine whether β2PIX was phosphorylated by PKCγ, we performed *in vitro*, in cells, and *in vivo* phosphorylation experiments. β2PIX was phosphorylated by PKCγ *in vitro*, whereas the inhibition of PKC activity with GFX abolished the phosphorylation (Fig. 3*A*). Next, we investigated whether β2PIX was phosphorylated by PKC in cells. Enhanced phosphorylation of FLAG-tagged β2PIX extracted from HEK293 cells transfected with FLAG-tagged β2PIX and GFP-tagged PKCγ after treatment with 1 μM TPA was observed with an anti-Ser PKC motif Ab (Fig. 3*B*). Furthermore, the TPA-induced phosphorylation of β2PIX in cells was reduced by the PKC inhibitors Gö6976 and GFX (Fig. 3*B*). These results were further confirmed in PC12 cells (Fig. 3*C*) and in the P2 synaptosomal fraction of the mouse brain (Fig. 3*D*). Collectively, these results showed that β2PIX was phosphorylated by Ca^{2+}-dependent PKC *in vitro*, in cells, and *in vivo*.

PKCγ phosphorylates Thr76 in SH3, Ser340 in PH, and Ser583 in the C terminus of β2PIX *in vitro*

β2PIX consists of the following four regions: SH3 (1–92 aa), DH (93–274 aa), PH (275–400 aa), and the C terminus (401–625 aa). Because each region of β2PIX contains one or more predicted PKC phosphorylation sites, we performed an MS analysis combined with an in vitro phosphorylation assay using full-length GST-tagged β2PIX for screening the phosphorylation sites by PKCγ. The *in vitro* PKC assay, followed by the MS analysis, revealed the phosphorylation of Thr76, Ser215, and Ser583 in addition to that of Ser340, which was revealed by the phosphoproteome analysis of PKCγ KO mice (Fig. 2*C*). Thr76, Ser215, and Ser340 are common sites in both β1 and β2PIX. However, Ser583 is found only in β2PIX. To examine the PKCγ-mediated phosphorylation of these sites, recombinant proteins were used in *in vitro* phosphorylation assays. Importantly, all domains of β2PIX were phosphorylated by PKCγ *in vitro*, but the SH3 and C-terminal domains were phosphorylated much more strongly than the DH and PH domains (Fig. 4*A*). For the next step, we generated recombinant mutant proteins in which each Ser or Thr residue was replaced with Ala (Thr76Ala in SH3, Ser215Ala in DH, Ser340Ala in PH, and Ser583Ala in the C terminus) and examined which Ser/Thr residues of Thr76, Ser215, Ser340, or Ser583 could be phosphorylated by PKCγ *in vitro*. We observed that the Thr76Ala and Ser583Ala mutant proteins exhibited impaired phosphorylation of the SH3 and C-terminal domains (Fig. 4*B*). The Ser340Ala in the PH domain showed a moderately reduced phosphorylation. The Ser215Ala showed no significant reduction of phosphorylation in the DH domain. These findings suggested that Thr76, Ser340, and Ser583, but not Ser215, are PKCγ phosphorylation sites *in vitro*.

cPKC phosphorylates β2PIX Ser340 and Ser583 in cells

To further confirm that β2PIX is phosphorylated by cPKC in cells, we produced Abs that specifically recognized phosphorylated Thr76, Ser340, and Ser583 (Fig. 4*C*). The purified full-length β2PIX was phosphorylated by recombinant PKCγ *in vitro* and then applied to SDS-PAGE, which was followed by Western blotting with the anti-pT76, anti-pS340, and anti-pS583 Abs. The β2PIX that was phosphorylated by PKCγ was detected by anti-pT76 and anti-pS583, but not the anti-pS340 Ab (Fig. 4*D*), suggesting that Ser340 was not a direct PKC phosphorylation site. Next, we investigated whether β2PIX was phosphorylated at Thr76, Ser340, and Ser583 in cells. Figure 5 shows that Ser340 and Ser583, but not Thr76, were phosphorylated in TPA-treated HEK293 cells. Moreover, the PKC-dependent phosphorylation of Ser340 and Ser583 was confirmed with the PKC inhibitors Gö6976 and GFX (Fig. 5). These findings suggested that Ser340 and Ser583 were phosphorylated by cPKC in cells. It is noteworthy that Ser583 was phosphorylated directly, whereas Ser340 was phosphorylated indirectly by PKCγ.

Involvement of cPKC in the regulation of DA release

A ^{3}H-DA release assay in PC12 cells, a cell line in a DAergic neuronal model, was used to study the functional role of PKC and βPIX in the regulation of DA release. PC12 cells expressed endogenous βPIXs and cPKCs, including PKCγ (Fig. 6*A*). To determine the degree of DA release stimulated by K^+, PC12 cells were stimulated with various K^+ concentrations and the DA release was increased in a K^+ concentration-dependent manner (Fig. 6*B*). The functional role of cPKC in the regulation of K^+-induced DA release was monitored with Gö6976 and GFX. These PKC inhibitors significantly decreased the high K^+-stimulated DA release (Fig. 6*C*). It is noted that there were no differences of ^{3}H-DA uptake into the PC12 cells between the control and PKC inhibitor groups (Fig. 6*D*,*E*). Gö6976 and GFX also significantly suppressed the TPA-stimulated DA release (Fig. 6*F*). The activation of PKCγ after K^+-induced depolarization was confirmed by monitoring the translocation of GFP-tagged PKCγ from the cytosol to the plasma membrane in PC12 cells (Fig. 7*A*). These

results suggested that cPKC plays a crucial role in K^+-induced DA release machinery in PC12 cells.

βPIX KD suppressed DA release

Because βPIX is able to stimulate growth hormone secretion from PC12 cells (Momboisse et al., 2009; Momboisse et al., 2010), we investigated the possible relationship between βPIX and DA release. KD of βPIX in PC12 cells by shRNA (sh369) resulted in a significant inhibition of K^+-evoked DA secretion from PC12 cells (Fig. 7*B*). A similar significant reduction in DA release was reproduced with synthetic βPIX siRNA (Fig. 7*C*). These results were consistent with the idea that βPIX is an important element of the DA exocytotic machinery.

PKC-mediated phosphorylation of β2PIX at Ser340 and Ser583 promoted DA release

To determine the role of the PKC-mediated phosphorylation of βPIX in DA release, we exogenously and simultaneously introduced the shRNA-resistant forms of β2PIX mutant, including β2PIX Thr76Ala, Ser340Ala, or Ser583Ala mutants and βPIX sh369, into PC12 cells. DA release from PC12 cells transfected with sh369 was completely rescued by the reintroduction of WT FLAG-tagged β2PIX (Fig. 8*A*). These results suggested that β2PIX, which is a dominant isoform in the CNS, has important roles in DA release. Moreover, we examined the effects of the β2PIX phosphorylation on DA release. β2PIX Ser340Ala and Ser583Ala mutants failed to rescue the reduced DA release by βPIX sh369, whereas the β2PIX Thr76Ala mutant acted similarly to WT β2PIX (Fig. 8*A*). Together, our results suggested that the PKC-mediated phosphorylation of Ser340 and Ser583 on β2PIX positively regulates DA release. Finally, we examined the effects of Cdc42 and Rac1 KD on DA release. When Cdc42 was knocked down, Rac1 was upregulated and vice versa. Therefore, we knocked down both Cdc42 and Rac1. The KD of both Cdc42 and Rac1 in PC12 cells by shRNAs resulted in a significant inhibition of K^+-evoked DA release from PC12 cells (Fig. 8*B*).

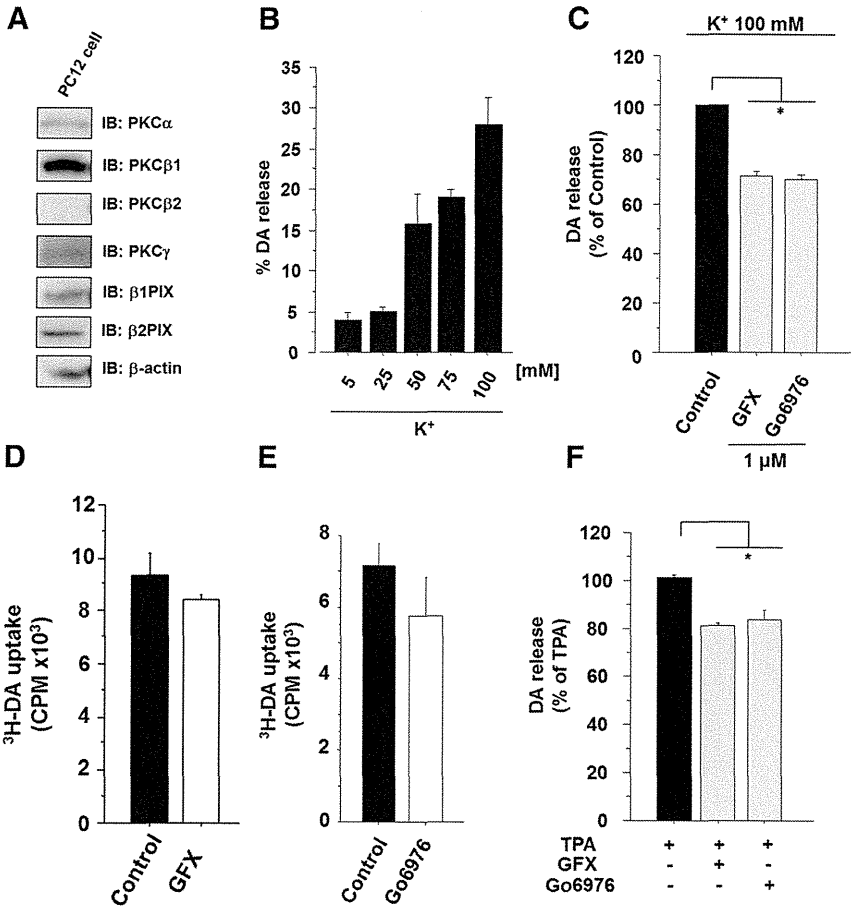

Figure 6. cPKC positively regulates K^+-stimulated DA release. ***A***, cPKCs and βPIX are expressed in PC12 cells. PC12 cell lysates were analyzed with immunoblotting with anti-PKCα, β1, β2, γ, and βPIX antibodies. ***B***, DA release in PC12 cells was measured with various K^+ concentrations. The results are expressed as mean ± SEM ($n = 3$). ***C***, Amounts of DA release that were stimulated in response to 100 mM K^+ with 1 μM GFX or 1 μM Gö6976 were measured in PC12 cells ($n = 3$; $^*p < 0.05$, unpaired *t* test). DA release levels were normalized to the levels released in response to 100 mM K^+, which were set to 100%. The results are expressed as mean ± SEM ($n = 3$–5). ***D***, ***E***, Uptake of ^{3}H-DA into PC12 cells with or without GFX and Gö6976 were measured. The results are expressed as mean ± SEM ($n = 3$). ***F***, TPA stimulated DA release in PC12 cells. DA release in PC12 cells was measured with 1 μM TPA in the absence or presence of 1 μM GFX. DA release levels were normalized to that of 1 μM TPA stimulation, which was set to 100%. The results are expressed as mean ± SEM ($n = 3$, $^*p < 0.01$, unpaired *t* test).

Discussion

In this study, we revealed that AS/AGU rats did not express full-length PKCγ or the truncated form of PKCγ, indicating that a loss, and not a gain, of function is the cause of the parkinsonian symptoms exhibited by AS/AGU rats. In agreement with these findings, we demonstrated decreased DA release stimulated by high levels of K^+ and METH in the striatum. It is noteworthy that altered DA release is the predominant characteristic of parkinsonian symptoms in PKCγ KO mice rather than loss of DAergic neurons in the SNpc. We propose that PKCγ KO animals are useful models for the study of parkinsonian syndrome because PKCγ KO mice and AS/AGU rats have damage not only in the DAergic system, but also in the serotonergic system (Al-Fayez et al., 2005), as has been observed in patients with sporadic Parkinson's disease. Furthermore, the use of the PKCγ KO mouse model has an advantage because it is possible to perform gene manipulations in them, such as PKCγ rescue, compared with the AS/AGU rats.

Although it is generally accepted that DA release in the striatum induced by high K^+ levels is mediated by exocytosis and not by DAT, PKC was reported to induce DAT endocytosis (Daniels and Amara, 1999), which, by altering DA reuptake, can change the amplitude of K^+-induced DA release as measured by microdialysis. We have ruled out this possibility because DAT activity was instead decreased in PKCγ KO mice (Fig. 1*F*). Moreover, ^{3}H-DA uptake does not differ between the control and PKC inhibitors in PC12 cells (Fig. 6*D*,*E*). These results suggested that the reduced K^+-induced DA release was not through the change of the DAT endocytosis by the PKCγ KO. There are also reports that activation of PKC induces DAT-mediated DA reverse transport (Kantor and Gnegy, 1998; Cowell et al., 2000). Although

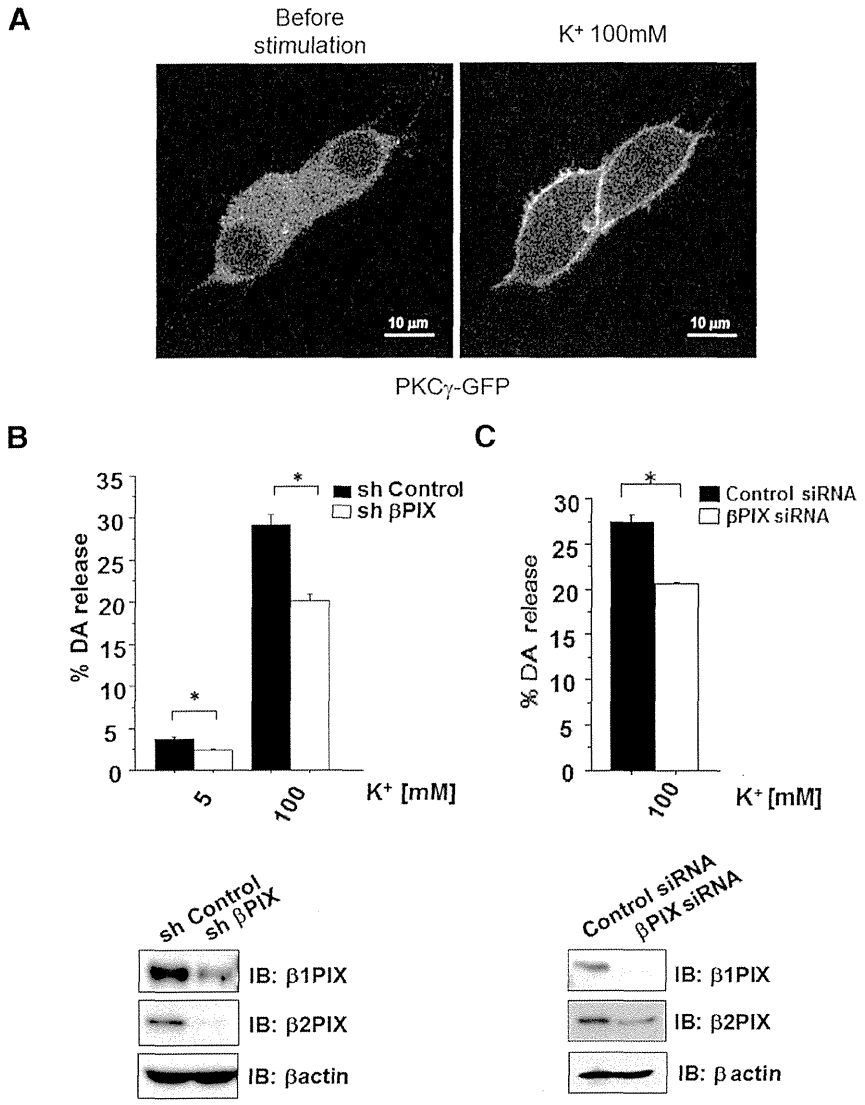

Figure 7. βPIX positively regulates K^+-stimulated DA release. ***A***, PKCγ was activated by high K^+ level stimulation in PC12 cells. Activation of PKCγ by K^+ stimulation was examined by monitoring the translocation of GFP-tagged PKCγ in PC12 cells. ***B***, DA release was measured in PC12 cells that were transfected with shRNA for βPIX and sh Control, which was used as a negative control. The results are expressed as mean ± SEM ($n = 6$, $^*p < 0.01$, *unpaired t* test). ***C***, DA release was measured in PC12 cells transfected with siRNA for βPIX. The expression of siRNAs for βPIX in PC12 cells and lysate was analyzed by immunoblot analyses with anti-βPIX antibodies. The results are expressed as mean ± SEM ($n = 5$, $^*p < 0.01$, unpaired *t* test).

these studies focused more on PKCβ than on PKCγ, our study showed that PKCγ also play important roles for DAT-mediated DA reverse transport (Fig. 1*F*), suggesting that PKCγ play roles for both K^+-mediated DA release and DAT-mediated DA reverse transport. Therefore, PKCγ KO resulted in decreased DAT activity, including uptaking DA and DA reverse transport through DAT. The decreased level of K^+-induced DA release in PKCγ KO mice is probably underestimated: DA release may be more significantly decreased when the disordered DAT activity is normalized.

We identified 10 phosphoproteins that were decreased in PKCγ KO mice under the hypothesis that decreased levels of phosphorylated substrates of PKCγ in the nigrostriatal system lead to impairments in DA release. Our results indicated that βPIX was one of the pivotal targets of PKCγ or cPKC in enhancing Ca^{2+}-evoked DA release based on the following several lines of evidence: (1) PKCγ phosphorylated βPIX *in vitro*, in cells, and *in vivo*; (2) Ser583 of βPIX was phosphorylated by PKCγ both *in vitro* and in cells, whereas Ser340 was phosphorylated by cPKC only in cells, suggesting that cPKC indirectly phosphorylated Ser340; (3) cPKC inhibitors and the KD of endogenous βPIX also suppressed the DA release from PC12 cells, suggesting that both PKCγ or cPKC and βPIX play pivotal roles in Ca^{2+}-evoked DA release from DAergic neurons; and (4) WT β2PIX, but not Ser340Ala or Ser583Ala, rescued the decreased DA release from PC12 cells by sh369 for βPIX, suggesting that both phosphorylation sites are necessary for regulating DA release. Why does PKCγ KO cause the parkinsonian syndrome phenotype, even when other cPKCs are expressed in PKCγ KO animals? Although the substrate specificity of each PKC subtype appears to be low *in vitro*, there have been several confirmatory reports of subtype-specific functions of cPKC under physiological conditions (Uchino et al., 2004; Ueyama et al., 2004; Al-Fayez et al., 2005; Kawasaki et al., 2010; Sakuma et al., 2012). Our data suggest that PKCγ has important roles in DA release in mice.

In neurons, Ca^{2+} entry triggers exocytosis, suggesting that certain Ca^{2+} sensors may be necessary for Ca^{2+}-dependent exocytosis. Candidates for Ca^{2+} sensors include molecules that possess EF hand motifs or C2 domains, which were first defined in cPKC, and annexin family proteins, as has been reported previously (Burgoyne and Morgan, 1998). PKC has been reported to modify exocytosis in the steps both before and after docking to the plasma membrane through the following mechanisms: (1) increased vesicle recruitment into the readily releasable pool (Gillis et al., 1996; Stevens and Sullivan, 1998), (2) acceleration of fusion pore expansion (Scepek et al., 1998), and (3) changes in the kinetics of exocytosis (Graham et al., 2002). However, βPIX is related to the exocytosis step after docking (Momboisse et al., 2009; Momboisse et al., 2010). The cPKC-βPIX-Cdc42/Rac1 axis possibly has important roles in DA release in the step after docking through the βPIX phosphorylation by cPKC.

How can βPIX regulate DA release through the phosphorylation at Ser340 or Ser583? Previous reports have revealed that βPIX phosphorylation results in βPIX translocation to the membrane and the subsequent activation of Rac1 and/or Cdc42. In PC12 cells, basic fibroblast growth factor induces the phosphorylation of βPIX at Ser525 and Thr526, resulting in neurite outgrowth by the activation of Rac1 through the translocation of the βPIX complex at neuronal growth cones (Shin et al., 2002; Shin et al., 2006). In human mesangial cells, endothelin-1 and cAMP inducers cause the PKA-dependent phosphorylation of βPIX at Ser516 and Thr526, resulting in cytoskeletal rearrangement by

the activation of Cdc42 through βPIX translocation (Chahdi et al., 2005). Therefore, βPIX may be differently phosphorylated in response to various stimuli and this may result in its stimulus-dependent specific targeting and Cdc42/Rac1 activation at the targeted sites. We have demonstrated for the first time that Ser583 is a PKCγ or cPKC phosphorylation site. Ser583 and the previously reported sites Ser516, Ser525, and Thr526 are all located in the C-terminal domain of βPIX and may have similar functions for the translocation and subsequent activation of Cdc42/Rac1. Phosphorylation at Ser340 is located in the PH domain, which interacts with phosphatidylinositol lipids within biological membranes (Wang and Shaw, 1995) and may also play important roles in the membrane targeting of βPIX. In fact, the PH domain has been reported to interact with PKC (Yao et al., 1994) and Cdc42 (Rossman et al., 2002) and it has been implicated in the regulation of the GEF activity of SOS (Ras-GEF; Karlovich et al., 1995) and p140Ras-GRF (Ras and Rac GEF; Buchsbaum et al., 1996). Therefore, through PH-domain-mediated membrane targeting and interaction, the cPKC-βPIX-Cdc42/Rac1 axis may act at specific membranes (Chen et al., 1997; Falasca et al., 1998; Maffucci and Falasca, 2001). Downstream of the βPIX phosphorylation, we speculate that Cdc42/Rac1 are the targets of phosphorylated βPIX, as suggested in previous studies (Shin et al., 2002; Shin et al., 2004; Chahdi et al., 2005; Shin et al., 2006). Although we have not proved a direct relationship between phosphorylated βPIX and Cdc42/Rac1, we speculate that βPIX phosphorylated by PKCγ regulates Cdc42/Rac1 functions based on our data that the double KD of Cdc42 and Rac1 resulted in decreased DA release (Fig. 8*B*).

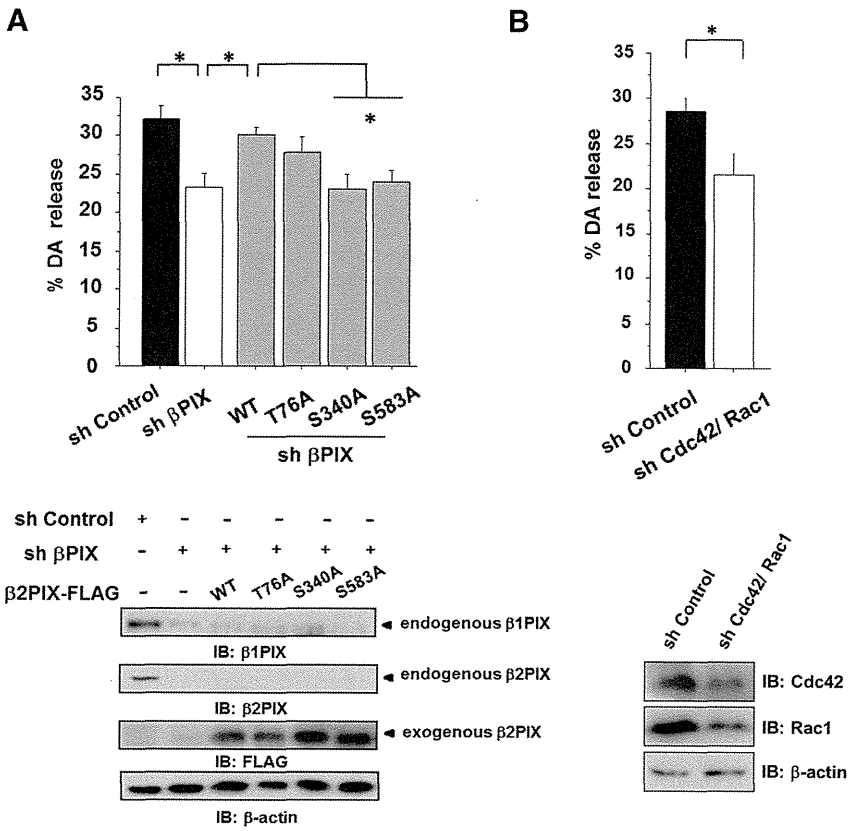

Figure 8. Phosphorylation of β2 PIX at Ser340 and Ser583 promotes DA release. ***A***, DA release was measured in PC12 cells that were transfected with shβPIX and β2PIX (WT and Ser-Ala mutants) with shRNA-resistant sequences. The levels of endogenous β1, β2PIX, and exogenous β2PIX were confirmed. Comparable levels of all ectopically expressed β2PIX proteins were confirmed by Western blot analyses. The results are expressed as mean ± SEM ($n = 3–6$, $^*p < 0.05$, one-way ANOVA with *post hoc* Dunnett's test). ***B***, DA release was measured in PC12 cells that were transfected with shRNA for both Cdc42 and Rac1 and sh Control, which was used as a negative control. The results are expressed as mean ± SEM ($n = 3$, $^*p < 0.01$, unpaired *t* test).

Although Ser340 is common to both β1PIX and β2PIX, Ser583 only exists in the unique C terminus of β2PIX, which is the neuron-dominant isoform (Koh et al., 2001) that emerged from and was conserved after *Xenopus laevis* (Fig. 9). Therefore, Ser583 phosphorylation by neuron-specific PKCγ may have important roles in the modulation of βPIX function in the highly developed CNS and highly elaborated function, including DA release. It is also of note that the reported phosphorylation sites at Ser340, Ser516, Ser525, and Thr526 are conserved through evolution. Although we detected the TPA-induced phosphorylation of β2PIX *in vivo* using the synaptosomal P2 fraction of PKCγ WT mice by pSer PKC motif Ab (Fig. 3*D*), we could not show clear TPA-induced phosphorylation at Ser340 and Ser583 in PKCγ WT using our site-specific phospho-Abs for pS340 and pS583, likely due to the sensitivity of anti-pS340 and pS583 Abs.

In the present study, we have demonstrated that PKCγ KO mice can be a useful model of parkinsonian syndrome. In addition, we found for the first time that DA release was positively regulated by the PKC-mediated direct phosphorylation of βPIX at Ser583 and indirect phosphorylation at Ser340. The phospho-

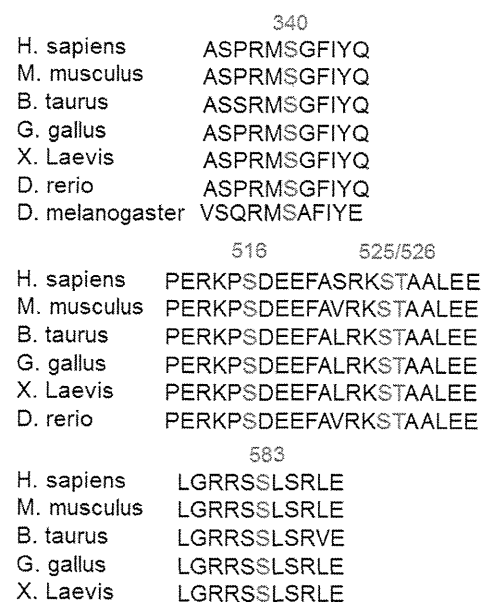

Figure 9. Schematic comparisons of Ser340 and Ser583 through evolution. Ser340 and Ser583 are evolutionally conserved in many species. It is noted that β2PIX emerged from *X. laevis*, although β1PIX is expressed in *Drosophila melanogaster*. Ser516, Ser525, and Thr526, as reported previously, are also conserved in many species.

rylational modulation of βPIX by PKCγ may be a potential therapeutic target for the treatment of parkinsonian syndrome.

References

Adachi N, Oyasu M, Taniguchi T, Yamaguchi Y, Takenaka R, Shirai Y, Saito N (2005) Immunocytochemical localization of a neuron-specific diacylglycerol kinase beta and gamma in the developing rat brain. Brain Res Mol Brain Res 139:288–299. CrossRef Medline

Ago Y, Araki R, Tanaka T, Sasaga A, Nishiyama S, Takuma K, Matsuda T (2013) Role of social encounter-induced activation of prefrontal serotonergic systems in the abnormal behaviors of isolation-reared mice. Neuropsychopharmacology 38:1535–1547. CrossRef Medline

Al-Fayez M, Russell D, Wayne Davies R, Shiels PG, Baker PJ, Payne AP (2005) Deficits in the mid-brain raphe nuclei and striatum of the AS/AGU rat, a protein kinase C-gamma mutant. Eur J Neurosci 22:2792–2798. CrossRef Medline

Audebert S, Navarro C, Nourry C, Chasserot-Golaz S, Lécine P, Bellaiche Y, Dupont JL, Premont RT, Sempéré C, Strub JM, Van Dorsselaer A, Vitale N, Borg JP (2004) Mammalian Scribble forms a tight complex with the betaPIX exchange factor. Curr Biol 14:987–995. CrossRef Medline

Barclay JW, Craig TJ, Fisher RJ, Ciufo LF, Evans GJ, Morgan A, Burgoyne RD (2003) Phosphorylation of Munc18 by protein kinase C regulates the kinetics of exocytosis. J Biol Chem 278:10538–10545. CrossRef Medline

Buchsbaum R, Telliez JB, Goonesekera S, Feig LA (1996) The N-terminal pleckstrin, coiled-coil, and IQ domains of the exchange factor Ras-GRF act cooperatively to facilitate activation by calcium. Mol Cell Biol 16:4888–4896. Medline

Burgoyne RD, Morgan A (1998) Calcium sensors in regulated exocytosis. Cell Calcium 24:367–376. CrossRef Medline

Campbell JM, Payne AP, Gilmore DP, Byrne JE, Russell D, McGadey J, Clarke DJ, Davies RW, Sutcliffe RG (1996) Neostriatal dopamine depletion and locomotor abnormalities due to the Albino Swiss rat agu mutation. Neurosci Lett 213:173–176. Medline

Chahdi A, Sorokin A (2008) Protein kinase A-dependent phosphorylation modulates beta1Pix guanine nucleotide exchange factor activity through 14–3-3beta binding. Mol Cell Biol 28:1679–1687. CrossRef Medline

Chahdi A, Miller B, Sorokin A (2005) Endothelin 1 induces beta 1Pix translocation and Cdc42 activation via protein kinase A-dependent pathway. J Biol Chem 280:578–584. CrossRef Medline

Chefer VI, Czyzyk T, Bolan EA, Moron J, Pintar JE, Shippenberg TS (2005) Endogenous kappa-opioid receptor systems regulate mesoaccumbal dopamine dynamics and vulnerability to cocaine. J Neurosci 25:5029–5037. CrossRef Medline

Chen RH, Corbalan-Garcia S, Bar-Sagi D (1997) The role of the PH domain in the signal-dependent membrane targeting of Sos. EMBO J 16:1351–1359. CrossRef Medline

Cowell RM, Kantor L, Hewlett GH, Frey KA, Gnegy ME (2000) Dopamine transporter antagonists block phorbol ester-induced dopamine release and dopamine transporter phosphorylation in striatal synaptosomes. Eur J Pharmacol 389:59–65. CrossRef Medline

Craig NJ, Durán Alonso MB, Hawker KL, Shiels P, Glencorse TA, Campbell JM, Bennett NK, Canham M, Donald D, Gardiner M, Gilmore DP, MacDonald RJ, Maitland K, McCallion AS, Russell D, Payne AP, Sutcliffe RG, Davies RW (2001) A candidate gene for human neurodegenerative disorders: a rat PKC gamma mutation causes a parkinsonian syndrome. Nat Neurosci 4:1061–1062. CrossRef Medline

Daniels GM, Amara SG (1999) Regulated trafficking of the human dopamine transporter: clathrin-mediated internalization and lysosomal degradation in response to phorbol esters. J Biol Chem 274:35794–35801. CrossRef Medline

Ding YQ, Xiang CX, Chen ZF (2005) Generation and characterization of the PKC gamma-Cre mouse line. Genesis 43:28–33. CrossRef Medline

Falasca M, Logan SK, Lehto VP, Baccante G, Lemmon MA, Schlessinger J (1998) Activation of phospholipase C gamma by PI 3-kinase-induced PH domain-mediated membrane targeting. EMBO J 17:414–422. CrossRef Medline

Feng Q, Baird D, Peng X, Wang J, Ly T, Guan JL, Cerione RA (2006) Cool-1 functions as an essential regulatory node for EGF receptor- and Src-mediated cell growth. Nat Cell Biol 8:945–956. CrossRef Medline

Franklin KBJ, Paxinos G (1997) The mouse brain in stereotaxic coordinates. San Diego: Academic.

Gillis KD, Mossner R, Neher E (1996) Protein kinase C enhances exocytosis from chromaffin cells by increasing the size of the readily releasable pool of secretory granules. Neuron 16:1209–1220. CrossRef Medline

Graham ME, O'Callaghan DW, McMahon HT, Burgoyne RD (2002) Dynamin-dependent and dynamin-independent processes contribute to the regulation of single vesicle release kinetics and quantal size. Proc Natl Acad Sci U S A 99:7124–7129. CrossRef Medline

Hewett J, Johanson P, Sharma N, Standaert D, Balcioglu A (2010) Function of dopamine transporter is compromised in DYT1 transgenic animal model in vivo. J Neurochem 113:228–235. CrossRef Medline

Hilfiker S, Pieribone VA, Nordstedt C, Greengard P, Czernik AJ (1999) Regulation of synaptotagmin I phosphorylation by multiple protein kinases. J Neurochem 73:921–932. CrossRef Medline

Iwasaki S, Kataoka M, Sekiguchi M, Shimazaki Y, Sato K, Takahashi M (2000) Two distinct mechanisms underlie the stimulation of neurotransmitter release by phorbol esters in clonal rat pheochromocytoma PC12 cells. J Biochem 128:407–414. CrossRef Medline

Justice JB Jr (1993) Quantitative microdialysis of neurotransmitters. J Neurosci Methods 48:263–276. CrossRef Medline

Kantor L, Gnegy ME (1998) Protein kinase C inhibitors block amphetamine-mediated dopamine release in rat striatal slices. J Pharmacol Exp Ther 284:592–598. Medline

Karlovich CA, Bonfini L, McCollam L, Rogge RD, Daga A, Czech MP, Banerjee U (1995) In vivo functional analysis of the Ras exchange factor son of sevenless. Science 268:576–579. CrossRef Medline

Kawasaki T, Ishihara K, Ago Y, Nakamura S, Itoh S, Baba A, Matsuda T (2006) Protective effect of the radical scavenger edaravone against methamphetamine-induced dopaminergic neurotoxicity in mouse striatum. Eur J Pharmacol 542:92–99. CrossRef Medline

Kawasaki T, Ishihara K, Ago Y, Baba A, Matsuda T (2007) Edaravone (3-methyl-1-phenyl-2-pyrazolin-5-one), a radical scavenger, prevents 1-methyl-4-phenyl-1,2,3,6-tetrahydropyridine-induced neurotoxicity in the substantia nigra but not the striatum. J Pharmacol Exp Ther 322:274–281. CrossRef Medline

Kawasaki T, Ueyama T, Lange I, Feske S, Saito N (2010) Protein kinase C-induced phosphorylation of Orai1 regulates the intracellular Ca^{2+} level via the store-operated Ca^{2+} channel. J Biol Chem 285:25720–25730. CrossRef Medline

Koda K, Ago Y, Cong Y, Kita Y, Takuma K, Matsuda T (2010) Effects of acute and chronic administration of atomoxetine and methylphenidate on extracellular levels of noradrenaline, dopamine and serotonin in the prefrontal cortex and striatum of mice. J Neurochem 114:259–270. CrossRef Medline

Koh CG, Manser E, Zhao ZS, Ng CP, Lim L (2001) Beta1PIX, the PAK-interacting exchange factor, requires localization via a coiled-coil region to promote microvillus-like structures and membrane ruffles. J Cell Sci 114:4239–4251. Medline

Kose A, Ito A, Saito N, Tanaka C (1990) Electron microscopic localization of gamma- and beta II-subspecies of protein kinase C in rat hippocampus. Brain Res 518:209–217. CrossRef Medline

Kyono Y, Sugiyama N, Imami K, Tomita M, Ishihama Y (2008) Successive and selective release of phosphorylated peptides captured by hydroxy acid-modified metal oxide chromatography. J Proteome Res 7:4585–4593. CrossRef Medline

Maffucci T, Falasca M (2001) Specificity in pleckstrin homology (PH) domain membrane targeting: a role for a phosphoinositide-protein co-operative mechanism. FEBS Lett 506:173–179. CrossRef Medline

Matsubara T, Ikeda M, Kiso Y, Sakuma M, Yoshino K, Sakane F, Merida I, Saito N, Shirai Y (2012) c-Abl tyrosine kinase regulates serum-induced nuclear export of diacylglycerol kinase α by phosphorylation at Tyr-218. J Biol Chem 287:5507–5517. CrossRef Medline

Mayhew MW, Jeffery ED, Sherman NE, Nelson K, Polefrone JM, Pratt SJ, Shabanowitz J, Parsons JT, Fox JW, Hunt DF, Horwitz AF (2007) Identification of phosphorylation sites in betaPIX and PAK1. J Cell Sci 120:3911–3918. CrossRef Medline

Momboisse F, Lonchamp E, Calco V, Ceridono M, Vitale N, Bader MF, Gasman S (2009) betaPIX-activated Rac1 stimulates the activation of phospholipase D, which is associated with exocytosis in neuroendocrine cells. J Cell Sci 122:798–806. CrossRef Medline

Momboisse F, Ory S, Ceridono M, Calco V, Vitale N, Bader MF, Gasman S (2010) The Rho guanine nucleotide exchange factors Intersectin 1L and β-Pix control calcium-regulated exocytosis in neuroendocrine PC12 cells. Cell Mol Neurobiol 30:1327–1333. CrossRef Medline

Murray D, Honig B (2002) Electrostatic control of the membrane targeting of C2 domains. Mol Cell 9:145–154. CrossRef Medline

Nishizuka Y (1988) The molecular heterogeneity of protein kinase C and its implications for cellular regulation. Nature 334:661–665. CrossRef Medline

Nishizuka Y (1992) Intracellular signaling by hydrolysis of phospholipids and activation of protein kinase C. Science 258:607–614. CrossRef Medline

Ota T, Suzuki Y, Nishikawa T, Otsuki T, Sugiyama T, Irie R, Wakamatsu A, Hayashi K, Sato H, Nagai K, Kimura K, Makita H, Sekine M, Obayashi M, Nishi T, Shibahara T, Tanaka T, Ishii S, Yamamoto J, Saito K, et al. (2004) Complete sequencing and characterization of 21,243 full-length human cDNAs. Nat Genet 36:40–45. CrossRef Medline

Payne AP, Campbell JM, Russell D, Favor G, Sutcliffe RG, Bennett NK, Davies RW, Stone TW (2000) The AS/AGU rat: a spontaneous model of disruption and degeneration in the nigrostriatal dopaminergic system. J Anat 196:629–633. CrossRef Medline

Rossman KL, Worthylake DK, Snyder JT, Siderovski DP, Campbell SL, Sondek J (2002) A crystallographic view of interactions between Dbs and Cdc42: PH domain-assisted guanine nucleotide exchange. EMBO J 21:1315–1326. CrossRef Medline

Saito H, Oda Y, Sato T, Kuromitsu J, Ishihama Y (2006) Multiplexed two-dimensional liquid chromatography for MALDI and nanoelectrospray ionization mass spectrometry in proteomics. J Proteome Res 5:1803–1807. CrossRef Medline

Saito N, Shirai Y (2002) Protein kinase C gamma (PKC gamma): function of neuron specific isotype. J Biochem 132:683–687. CrossRef Medline

Sakuma M, Shirai Y, Yoshino K, Kuramasu M, Nakamura T, Yanagita T, Mizuno K, Hide I, Nakata Y, Saito N (2012) Novel PKCα-mediated phosphorylation site(s) on cofilin and their potential role in terminating histamine release. Mol Biol Cell 23:3707–3721. CrossRef Medline

Scepek S, Coorssen JR, Lindau M (1998) Fusion pore expansion in horse eosinophils is modulated by Ca^{2+} and protein kinase C via distinct mechanisms. EMBO J 17:4340–4345. CrossRef Medline

Seki T, Adachi N, Ono Y, Mochizuki H, Hiramoto K, Amano T, Matsubayashi H, Matsumoto M, Kawakami H, Saito N, Sakai N (2005) Mutant protein kinase Cgamma found in spinocerebellar ataxia type 14 is susceptible to aggregation and causes cell death. J Biol Chem 280:29096–29106. CrossRef Medline

Shin EY, Shin KS, Lee CS, Woo KN, Quan SH, Soung NK, Kim YG, Cha CI, Kim SR, Park D, Bokoch GM, Kim EG (2002) Phosphorylation of p85 beta PIX, a Rac/Cdc42-specific guanine nucleotide exchange factor, via the Ras/ERK/PAK2 pathway is required for basic fibroblast growth factor-induced neurite outgrowth. J Biol Chem 277:44417–44430. CrossRef Medline

Shin EY, Woo KN, Lee CS, Koo SH, Kim YG, Kim WJ, Bae CD, Chang SI, Kim EG (2004) Basic fibroblast growth factor stimulates activation of Rac1 through a p85 betaPIX phosphorylation-dependent pathway. J Biol Chem 279:1994–2004. CrossRef Medline

Shin EY, Lee CS, Cho TG, Kim YG, Song S, Juhnn YS, Park SC, Manser E, Kim EG (2006) betaPak-interacting exchange factor-mediated Rac1 activation requires smgGDS guanine nucleotide exchange factor in basic fibroblast growth factor-induced neurite outgrowth. J Biol Chem 281:35954–35964. CrossRef Medline

Stevens CF, Sullivan JM (1998) Regulation of the readily releasable vesicle pool by protein kinase C. Neuron 21:885–893. CrossRef Medline

ten Klooster JP, Jaffer ZM, Chernoff J, Hordijk PL (2006) Targeting and activation of Rac1 are mediated by the exchange factor beta-Pix. J Cell Biol 172:759–769. CrossRef Medline

Uchino M, Sakai N, Kashiwagi K, Shirai Y, Shinohara Y, Hirose K, Iino M, Yamamura T, Saito N (2004) Isoform-specific phosphorylation of metabotropic glutamate receptor 5 by protein kinase C (PKC) blocks Ca^{2+} oscillation and oscillatory translocation of Ca^{2+}-dependent PKC. J Biol Chem 279:2254–2261. CrossRef Medline

Ueyama T, Lennartz MR, Noda Y, Kobayashi T, Shirai Y, Rikitake K, Yamasaki T, Hayashi S, Sakai N, Seguchi H, Sawada M, Sumimoto H, Saito N (2004) Superoxide production at phagosomal cup/phagosome through βI protein kinase C during FcγR-mediated phagocytosis in microglia. J Immunol 173:4582–4589. CrossRef Medline

Ueyama T, Geiszt M, Leto TL (2006) Involvement of Rac1 in activation of multicomponent Nox1- and Nox3-based NADPH oxidases. Mol Cell Biol 26:2160–2174. CrossRef Medline

Ueyama T, Sakaguchi H, Nakamura T, Goto A, Morioka S, Shimizu A, Nakao K, Hishikawa Y, Ninoyu Y, Kassai H, Suetsugu S, Koji T, Fritzsch B, Yonemura S, Hisa Y, Matsuda M, Aiba A, Saito N (2014) Maintenance of stereocilia and apical junctional complexes by Cdc42 in cochlear hair cells. J Cell Sci 127:2040–2052. CrossRef Medline

Wang DS, Shaw G (1995) The association of the C-terminal region of beta I sigma II spectrin to brain membranes is mediated by a PH domain, does not require membrane proteins, and coincides with a inositol-1,4,5 triphosphate binding site. Biochem Biophys Res Commun 217:608–615. CrossRef Medline

Wu WC, Walaas SI, Nairn AC, Greengard P (1982) Calcium/phospholipid regulates phosphorylation of a Mr "87k" substrate protein in brain synaptosomes. Proc Natl Acad Sci U S A 79:5249–5253. CrossRef Medline

Yao L, Kawakami Y, Kawakami T (1994) The pleckstrin homology domain of Bruton tyrosine kinase interacts with protein kinase C. Proc Natl Acad Sci U S A 91:9175–9179. CrossRef Medline

Association of the ASCO Classification with the Executive Function Subscores of the Montreal Cognitive Assessment in Patients with Postischemic Stroke

Kazuo Washida, MD, PhD,* Masafumi Ihara, MD, PhD,† Hisatsugu Tachibana, MD,* Kenji Sekiguchi, MD, PhD,* Hisatomo Kowa, MD, PhD,* Fumio Kanda, MD, PhD,* and Tatsushi Toda, MD, PhD*

Background: The ASCO classification can evaluate the etiology and mechanisms of ischemic stroke more comprehensively and systematically than conventional stroke classification systems such as Trial of Org 10172 in Acute Stroke Treatment (TOAST). Simultaneously, risk factors for cognitive impairment such as arterial sclerosis, leukoaraiosis, and atrial fibrillation can also be gathered and graded using the ASCO classification. *Methods:* Sixty patients with postischemic stroke underwent cognitive testing, including testing by the Japanese version of the Montreal cognitive assessment (MoCA-J) and the mini-mental state examination (MMSE). Ischemic strokes were categorized and graded by the ASCO classification. In this phenotype-based classification, every patient is characterized by the A-S-C-O system (A for Atherosclerosis, S for Small vessel disease, C for Cardiac source, and O for Other cause). Each of the 4 phenotypes is graded 0, 1, 2, or 3, according to severity. The conventional TOAST classification was also applied. Correlations between individual MoCA-J/MMSE scores and the ASCO scores were assessed. *Results:* The total score of the ASCO classification significantly correlated with the total scores of MoCA-J and MMSE. This correlation was more apparent in MoCA-J than in MMSE, because MoCA-J scores were normally distributed, whereas MMSE scores were skewed toward the higher end of the range (ceiling effect). Results for individual subtests of MoCA-J and MMSE indicated that cognitive function for visuoexecutive, calculation, abstraction, and remote recall significantly correlated with ASCO score. *Conclusions:* These results suggest that the ASCO phenotypic classification of stroke is useful not only for assessing the etiology of ischemic stroke but also for predicting cognitive decline after ischemic stroke. **Key Words:** ASCO phenotypic classification—poststroke cognitive impairment—Montreal cognitive assessment—mini-mental state examination.

The burden of stroke stemming from its effect on cognition has been underestimated for a long time. Ischemic stroke is a major cause of adult chronic disability and represents an important cause of cognitive decline and dementia. Poststroke cognitive impairment (PSCI) appears in about one third of patients with stroke.[1] The prevalence of cognitive impairment among patients with a history of stroke is similar to that of subjects

From the *Division of Neurology, Graduate School of Medicine, Kobe University, Kobe; and †Department of Neurology, The National Cerebral and Cardiovascular Center, Suita, Osaka, Japan.

Received March 25, 2014; accepted April 3, 2014.

This work was supported by a Grant-in-Aid for Scientific Research on Priority Areas from the Japanese Ministry of Education, Science and Culture (to T.T.).

Address correspondence to Kazuo Washida, MD, PhD, Division of Neurology, Kobe University, Graduate School of Medicine, Kusunoki-cho 7-5-2, Chuo-ku, Kobe 650-0017, Japan. E-mail: washida@med.kobe-u.ac.jp.

1052-3057/$ - see front matter

http://dx.doi.org/10.1016/j.jstrokecerebrovasdis.2014.04.009